Journal of Volcanology and Geothermal Research 255 (2013) 57–78

Contents lists available at SciVerse ScienceDirect

Journal of Volcanology and Geothermal Research

journal homepage: www.elsevier.com/locate/jvolgeores

Origin of the Düvertepe kaolin–alunite deposits in Simav Graben, Turkey: Timing and styles of hydrothermal mineralization

Ömer I. Ece [a,b,*], Bala Ekinci [a], Paul A. Schroeder [b], Douglas Crowe [b], Fahri Esenli [a]

[a] Istanbul Technical University (ITU), Faculty of Mines, Department of Geological Sciences, Maslak 34469, Istanbul, Turkey
[b] The University of Georgia (UGA), Department of Geology, Athens, GA 30602-2501, USA

ARTICLE INFO

Article history:
Received 6 June 2012
Accepted 23 January 2013
Available online 31 January 2013

Keywords:
Rhyolite–dacite volcanism
Acid-sulfate hydrothermal alteration
Extensional tectonism
Hypogene origin
Aegean graben system

ABSTRACT

The Düvertepe district located on the western end of the Simav Graben is the largest known fossil hydrothermal kaolin deposit in Turkey. Active hot springs occur to the north of Simav city (Eynal, Çitgöl, Naşa) and geothermal fields occur to the west of the graben (Hisaralan). Kaolin in the Düvertepe district formed at the expense of Miocene rhyolites–rhyodacites and tuffs emplaced in a tectonically active system undergoing N–S extension. Upward fan-shaped deposits of silicification and kaolin are found along fault zones and define areas of enhanced kaolinization. Silica sinters located above the kaolin zones suggest that hydrothermal fluids followed the fracture systems and mark outflow of geothermal waters. Fractured volcanic rocks rich in glass shards bear sufficient porosity and permeability for hydrothermal circulation. Two mineral facies, "kaolinite and alunite" dominate the deposits, which respectively include: (1) kaolinite–alunite–quartz and (2) alunite–opal-CT–quartz–halloysite. Kaolinite crystals are well-formed hexagonal vermiform habits and alunite crystals are idiomorphic rhombohedral forms. Needle- and tubular-shaped halloysites are common in the alunite facies. The $\delta^{34}S$ values for alunite range from −1.55 to +6.18‰. Kaolinites have δD ranging from −49.0 to −94.3‰ and the $\delta^{18}O$ values range from +5.8 to +14.8‰. Calculated formation temperatures of kaolin mineralization (using $\delta^{18}O$ values) suggest that hydrothermal alteration occurred in the range of 38° to 129 °C. Independent K/Ar and $^{40}Ar/^{39}Ar$ ages of alunite are concordant and indicate that alteration occurred from 20.1 to 20.6 Ma in the southern part of the graben and 17.3 to 19.2 Ma in the northern part. These results suggest that metasomatism by steam-heated hydrothermal fluids sourced by rhyolitic magma is responsible for the Düvertepe kaolin and alunite deposit origins.

1. Introduction

Many epithermal mineralizations in different sizes and chemical compositions observed along the Simav Graben were formed associated with two main tectono-magmatic periods during the tectonic and magmatic evolution of Western Anatolia (Oygür and Erler, 2000). N–S trending young transform faults cut through main south graben fault after the tectonic evolution of the Simav Graben. Large number of epithermal mineralizations observed along the tectonically active Simav Graben, occurred mostly along these transform faults, and Düvertepe kaolin (±alunite) and Şaphane alunite (±kaolin) deposits are two largest examples of this type of mineralizations (Fig. 1). Kaolin (±alunite) deposits occurred in the east and west ends of the Simav Graben as the result of acid sulfate geothermal waters (Mutlu et al., 2005).

The Simav Graben is a 150 km linear structure that trends WNW–ESE in central western Turkey (Fig. 1). The Simav Graben contains both modern and fossil-alteration evidence for a long and complex history of tectonism and hydrothermal activity; however field relations and the chronology of alteration events are poorly constrained. The Simav Graben is a Pliocene (?)–Quaternary structure which clearly cuts the NE–SW trending Demirci, Selendi and Akdere basins (Seyitoğlu, 1997). The south side of the graben is bounded by the north dipping listric Simav Fault. The Simav Graben is regarded as one of the latest products of N–S extensional tectonics, which began to affect the Aegean region in Latest Oligocene–Early Miocene times (Seyitoğlu, 1997). The graben hosts the Düvertepe kaolin district to the west and is currently one of the largest suppliers of material for regional ceramic and cement industries (Demirhan, 1986). The Şaphane kaolin district to the east also hosts varying amounts of alunite and siliceous deposits (Mutlu et al., 2005). Miocene rifting and associated rhyolitic (K-rich) volcanism resulted in the deposition of pyroclastic material in the central Simav Graben, Şaphane area (Snellings et al., 2008; Dilek and Altunkaynak, 2010). The Simav Graben region is tectonically active today (Oygür, 1997; Oygür and Erler, 2000; Altunkayanak and Dilek, 2006) and hot spring outflows are present north and east of Simav city and in

* Corresponding author at: Istanbul Technical University (ITU), Faculty of Mines, Department of Geological Sciences, Maslak 34469, Istanbul, Turkey. Tel./fax: +90 212 285 62 79.
E-mail address: ece@itu.edu.tr (Ö.I. Ece).

0377-0273/$ – see front matter © 2013 Elsevier B.V. All rights reserved.
http://dx.doi.org/10.1016/j.jvolgeores.2013.01.012

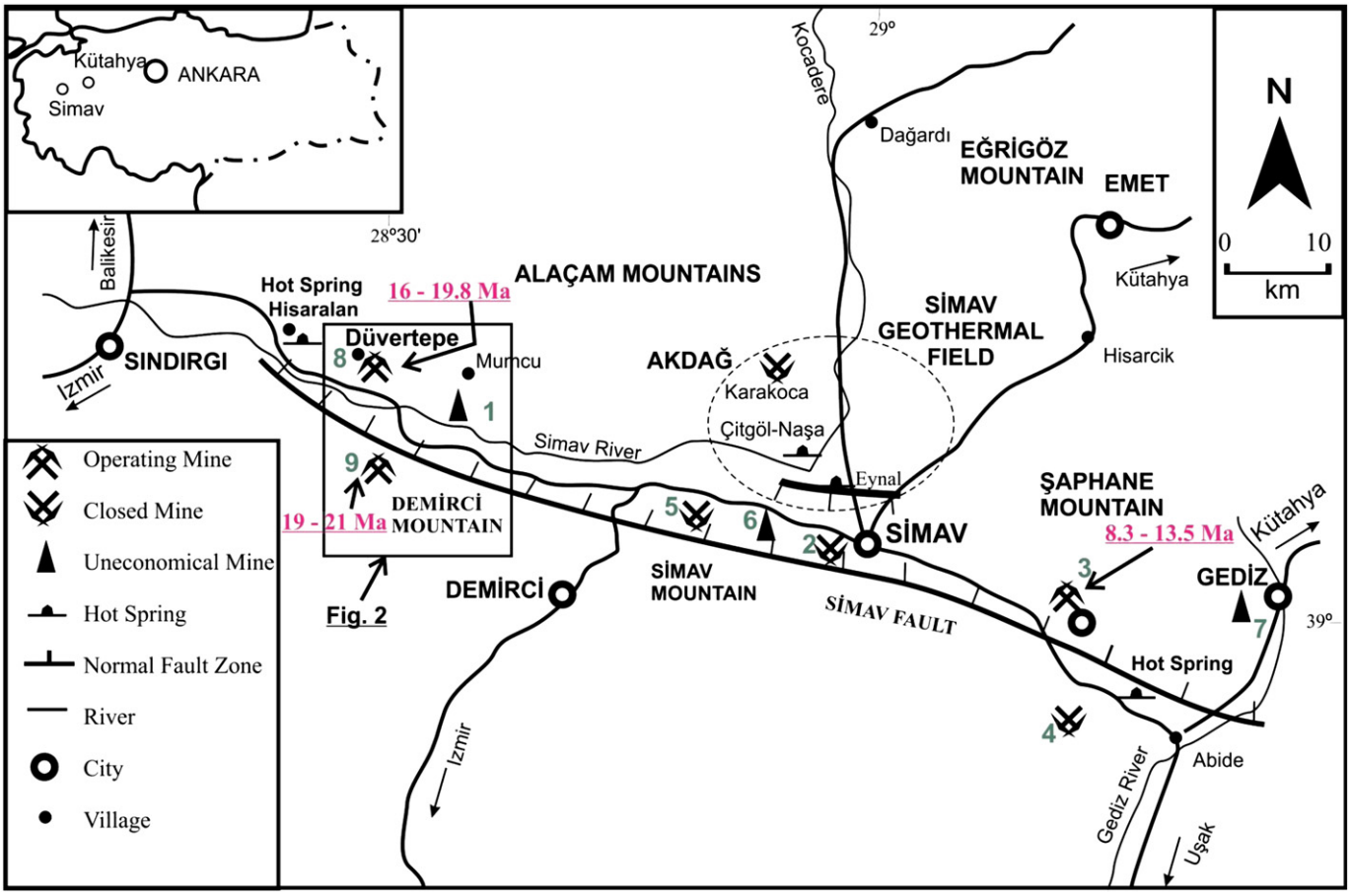

Fig. 1. Index map of the Simav Graben and location of the study area (Modified after Palabiyik and Serpen, 2008). Numbers indicate locations of epithermal deposits; (1) Mumcu — Au–Hg, (2) Degirmenciler — Sb, (3) Saphane — alunite–kaolinite, (4) Korkuyu — Sb–Hg, (5) Inkaya — Cu–Pb–Zn, (6) Arpacukuru — FeS_2, (7) Pinarbasi — Cu–Mo (Oygür and Erler, 2000); (8) Düvertepe — kaolinite–alunite and (9) Arpatarla–Sapci — kaolinite–alunite. Dates on the map are Ar–Ar model age from alunite samples.

Hisaralan, farther west of the Düvertepe district (Fig. 1). There are many high sulfidation epithermal kaolin deposits in the Düvertepe district situated in silicified zones as a consequence of hydrothermal alteration associated with fracture systems. There are also low sulfidation epithermal metal-bearing (FeS_2, $CuFeS_2$, PbS, ZnS, HgS, Sb_2S_3, MoS_2 and Au) zones along the Simav Graben, although these trends are not economically significant, their presence is consistent with a mixed alteration history. The total kaolin reserve in the Düvertepe district is approximately 20 million t with current annual production of 400,000 t/y. There is also minor production of $Al_2(SO_4)_3$ from alunite in the Şaphane area.

The purpose of this study is to provide a more detailed geologic map of the Düvertepe district, to clarify the conditions responsible for the genesis of kaolin and alunite, and to constrain the timing of hydrothermal alteration stages. Mineralogical and stable and radiogenic isotope investigations are used to evaluate the temporal and geochemical pathways that led to the formation of the deposit. A conceptual model is proposed herein to explain the origin of these deposits, which is then contrasted with similar epithermal deposits that occur around the world.

2. Geological framework

The Cenozoic tectonics of Turkey are characterized by the continental collision between Eurasian and Arabian plates resulting in continuous crustal thickening and shortening in Eastern Anatolia. N–S compression became active during Late Oligocene–Early Miocene in the Aegean Region (Seyitoğlu and Scott, 1992; Seyitoğlu, 1997) and N–S extensional tectonism accelerated with pulses in the Early–Middle Miocene and Plio-Quaternary (Dilek et al., 2009; Çoban et al., 2012; Altunkaynak et al., 2012). The Anatolian Block is moving westward along the North Anatolian Fault (NAF) zone (Okay et al., 1999) and causing N–S extension due to E–W compression (Okay et al., 2000). Following Late Cretaceous to Early Eocene compressive deformation, Western Anatolia hosted low-K to high-K calc-alkaline and medium-K to high-K alkaline magmas (Altunkayanak and Dilek, 2006; Akay, 2008; Altunkaynak and Genç, 2008; Dilek and Altunkaynak, 2010). The Early to Middle Miocene period was characterized by the appearance of almost contemporaneous alkaline and calc-alkaline magmas in a post-collisional intra-plate (back-arc) extensional setting. NE–SW *en-echelon* faults constitute the western end segments of the NAF zone in NW Turkey.

During the Early Miocene, wide areas were covered by andesite, dacite and rhyolite, with several large granodiorite plutons emplaced as shallow intrusions (Siyako et al., 1989). Calc-alkaline volcanism largely ceased during the Late Miocene. With the inception of the NAF later in the Miocene a large number of NE–SW trending dextral faults formed in the Biga Peninsula, all of which are still active today (Siyako et al., 1989; Okay et al., 1991) (ESM—Fig. 1) (Electronic Supplementary Material). There are two different views about the timing and mechanism for generation of the western Anatolian graben system. Some suggest that grabens developed during the Early Miocene (Şengör, 1985; Seyitoğlu and Scott, 1992), whereas others postulate a N–S extensional regime and associated basin formation during the Late Miocene to Early Pliocene (Görür et al., 1995; Yılmaz et al., 2000; Bozkurt, 2001; Dilek et al., 2009). By the end of the Late Miocene most workers agree that the N–S extension was interrupted by an erosional period and that E–W trending major graben basins formed (van Hinsbergen et al., 2010; Çoban et al., 2012). Approximately, ten E–W trending grabens currently exist, which include the Edremit, Bergama,

Gökova, Büyük Menderes, Küçük Menderes, Simav, and Gediz grabens. Their basin-bounding active normal faults are the most prominent structural and morphological features of the Western Turkey (Yılmaz et al., 2000; Bozkurt, 2001; Dilek et al., 2009; van Hinsbergen et al., 2010).

3. Local geology and petrography

Geological and stratigraphic relationships of the lithologic units in the Simav Graben and the Düvertepe kaolin district are shown in Fig. 2. The basement consists of Paleozoic metamorphic rocks, which are thought to be a part of a mélange series described by Akdeniz and Konak (1979) and Uz (1985). Mesozoic mélange exposures consist of metagraywacke, calc-schist, serpentine-schist, large limestone blocks, mudstone, and diabase dykes, which range individually up to tens of meters in thickness. Diabase dike lenses range from green to claret red in color and occur with the best exposures found west of the study area.

Early–Middle Miocene volcanics include rhyolitic–rhyodacitic tuffs, rhyolites, rhyolitic–rhyodacites, pumice rich rhyolitic–rhyodacitic tuffs, perlite and silicious rock bodies throughout the sequence. Pumice-rich rhyolitic tuffs are exposed between the Mezar Tepe and Şadırvan area, near Bağkıran and Arpatarla hills. Small to large (up to 5 mm) pumice fragments are white, dirty white, beige, pinkish, and yellowish beige. Petrographic studies show that rhyolitic tuffs display partial glassy and crystalline network textures.

The largest kaolin reserves are hosted within Early Miocene rhyolite–rhyodacite tuffs, which also have widespread occurrence in the study area. Good exposures of rhyolite–rhyodacite tuffs are found to the southeast in Cehennem Çukuru (Fig. 2) and Arpatarla Hill and to the southwest, north of Yaylabayır. Silicified rhyolite–rhyodacite tuff units are observed in southeast area. These tuffs are generally white and grade to gray at the base, greenish gray at the middle, and dark green at the top of the exposures. Kaolinization is observed between rhyolite–rhyodacite tuffs and above the silicious rock bodies in Arpatarla deposit. Vitric–crystalline rhyolite–rhyodacite tuffs contain a few rock fragments. The rock samples are made of vitric–crystalline matrix and phenocrysts are quartz, alkaline feldspar and subordinate mica (<1%).

Lower Miocene rhyolites are exposed south of Düvertepe village, north of Simav Graben (Fig. 2). These rocks have porphyritic texture and are semi-glassy to semi-crystalline. They are pinkish, reddish-pink, and white and are composed of fine-grained quartz, feldspar, biotite, and glassy groundmass. Spherules and volcanic gas vugs are found parallel to flow direction. The phenocrysts constitute about 40–50 vol.% of the rock. The mineral assemblage is made of semi-rounded quartz and altered alkaline feldspar (subhedral shape sanidine), and lesser amount (about 1–2 vol.%) of platy biotites (up to 3 mm) that are lineated parallel to flow direction. Opaque minerals are widely disseminated throughout the rocks.

Exposures of rhyodacite–dacites are found in the northwest (Baykuşçakılı), in southeast (Devletlibaba) and southwest. These rocks contain beige–bordeaux coarse-grained plagioclase. They are more siliceous and highly altered than the Devletlibaba and southwest areas due to surface weathering. These rocks have spherulite structures appearing both semi-glassy and semi-crystalline; which constitute more than 50% of the rock. Matrix is made of volcanic glass including plagioclase, biotite, and minor amount of quartz, K-feldspar and amphibole phenocrystals. Volcanic glass matrix, which is characterized by flow and spherulitic structures, is widely distributed in the rocks and

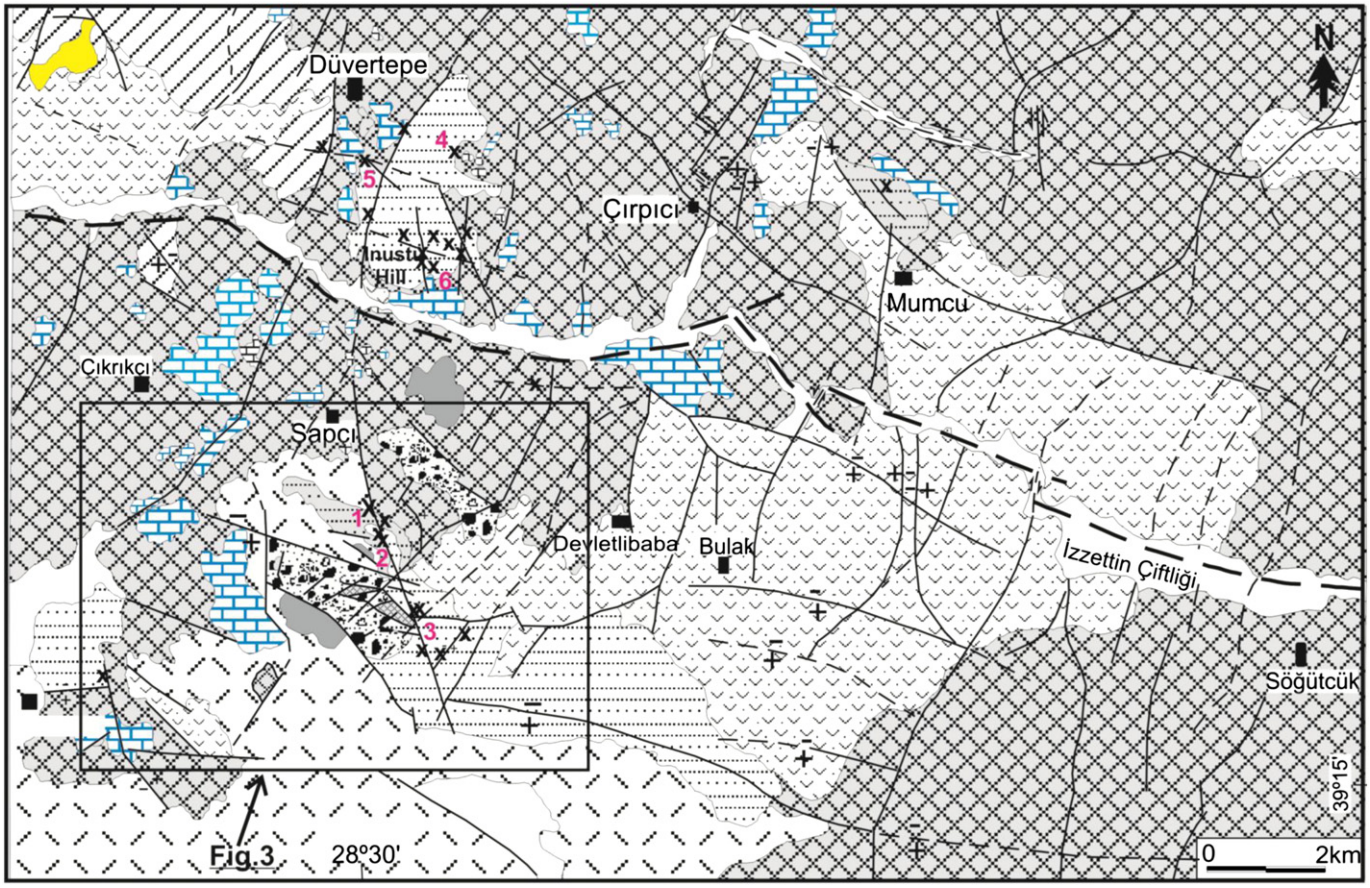

Fig. 2. Geologic map of the area of study (1/25,000 scale) at the Düvertepe district, Balıkesir. Solid lines show fault zone with relative displacement (±) and arrows indicate strike–slip fault zone along the Simav graben, where Simav River flows. Location of open and closed quarries shown with **X** symbol to reflect areas of fossil hydrothermal alterations. Numbers show the following kaolin quarries (1) Sapci, (2) Arpatarla, (3) Cennet Cukuru, (4) Doren, (5) Düvertepe and (6) bentonite quarries. Legend for map units is given in Fig. 3.

plagioclase is zoned. Opaque minerals are widely observed. Based on optical extinction angle measurements, plagioclase minerals have andesine composition. Sanidine minerals have broken fragment type appearance and iron oxide coatings.

Perlite and perlitic tuffs are exposed in northwest area, north of Simav Graben. Perlite blocks vary from 0.5 to 3 m within the tuffs. Glassy rhyolites (obsidian) are black and grayish-black, laminated and exhibit flow current marks. The interiors of white feldspar spheres contain secondary minerals. Laminated and bedded flow structures containing glassy rhyolite reach thickness of several meters that contain 70–80% glass matrix and 20–30% coarse phenocrysts. Phenocrysts exhibit both idiomorphic and hypoidiomorphic textures and display partly broken fragments. Phenocrysts are quartz (10–15%), plagioclase (generally oligoclase 5–8%), biotite (4–5%) and opaque minerals (1–2%).

Silicified rocks have type localities northeast of Şapçı, Kabaağaçlı, and Arpatarlası Hills. Some of these outcrops are exposed as large blocks and some others formed close to fault zones. Blocks are greenish-gray, very hard, and massive and have cryptocrystalline texture. In Kıranharmanı, silica content decreases from the outside to the inside of the exposures. Generally, the thickness of siliceous zone is less than 1 m in Çaltılıtaban, but in Kıranharmanı they vary from 1 to 50 m siliceous rocks near Karaağaçlı Hill. Primarily volcanic glass matrix totally transformed to silica minerals; these are micro and less abundant macro quartz (95–96%). Phenocrystals are made of feldspar (2–3%) and rare amount of opaque minerals and biotites (1–2%).

4. Düvertepe district kaolinite and alunite occurrences

The samples were collected from three kaolin quarries, located to the south of the southern graben limb and a fourth to the north of the southern limb (Fig. 2). The southern fault limb of Simav Graben has been active since Lower Miocene and it is still active today (there was an earthquake with a magnitude of 5.9 at May 19th, 2011). The northern fault limb is buried underneath sedimentary rocks and is currently thought to be passive (ESM—Fig. 1) (Electronic Supplementary Material). Brief descriptions of the respective quarry sites are found below.

4.1. Şapçı–Arpatarla kaolin deposits (south of graben)

Several kaolin deposits hosted by rhyolitic tuffs and rhyolites along the west side of NW–SE trending fault zone are situated about 2 km south of Şapçı (Fig. 2). Mineralization occurs on the west side of NNW–SSE trending main fault zone, which cuts through the Simav Graben. Quarry highwall and core drilling data indicate that the base of deposits is about 125 m below ground surface and that the thickness of kaolin zone varies from 10 to 20 m. Main mineral composition of the southern part of the Düvertepe kaolin occurrences is kaolinite, quartz and alunite. In addition to the presence of disseminated quartz, silica is mostly concentrated as opal nodules and cobbles in kaolin zones. Silica sinters are present above the kaolin deposit along major fault zone, especially in areas of Arpatarlası and Kabaağaçlı Hills (Fig. 3). Upward fan-shaped silicification along fault zones formed where hydrothermal fluids passed through the kaolin deposits, which demonstrates the structural control of the deposits (Fig. 3). Alunite is commonly found with heterogeneous distribution. The veins are rich in silica and alunite relative to kaolin zones. Several meters below the ground surface, kaolinization is about 10 m thick and contains up to ~30% Al_2O_3, <1% SO_4 and relatively low silica. Above there is a high silica (80% SiO_2), low kaolin (~10% Al_2O_3) and 2–5% SO_4. General views of kaolin quarries, fault relations and an overview of the study area are shown in Fig. 4.

4.2. Düvertepe–Moren kaolin deposits (north of graben)

To the north, the Moren kaolin quarry is located approximately 5 km from the Düvertepe village and contains kaolins that were formed inside rhyolite–ryhodacite tuffs along two small fault zones. The Moren quarry contains mostly kaolinite as the principal clay mineral. Quartz and silicified rock fragments are observed as accessory phases. The deposit exhibits two silica-rich fault zones with high quality kaolin between these faults. Drilling data indicate that the thickness of kaolin

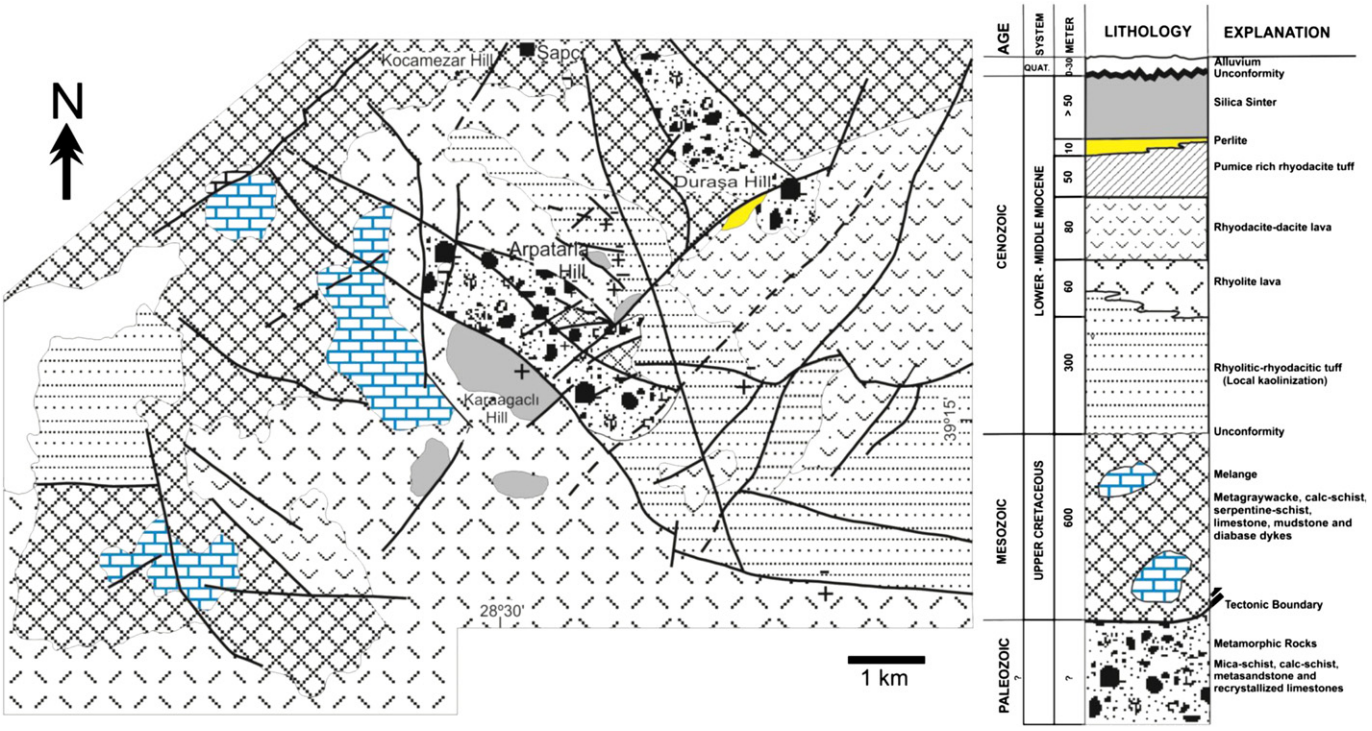

Fig. 3. Enlarged geological map of the biggest kaolin quarry (1/10,000 scale) in Şapçı–Arpatarla area and surroundings, south of Simav Graben.

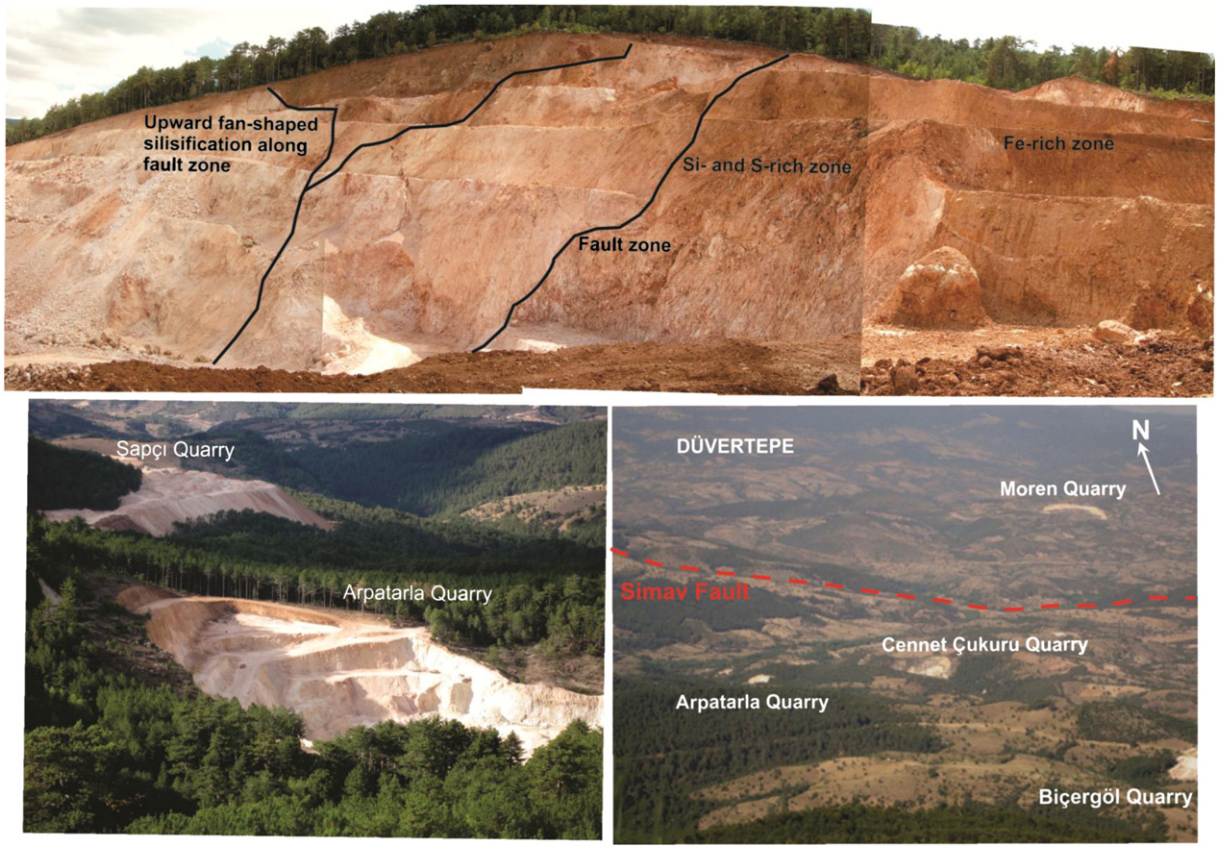

Fig. 4. The upper photo illustrates general view of highwalls in the Arpatarla kaolin quarry, south of the graben. The lower left shows general views of two major quarries and lower right are taken from the south of graben illustrating sight view of the study area.

zones ranges from 10 to 40 m and a smaller number of faults to the north. The kaolin deposit is smaller than those at the south and alunite is more common in north. Nearly pure alunite mineralization occurs in Inüstü Hill (Fig. 2), next to a fault zone, where halloysite is the only kaolin group mineral within this deposit. Small fault zone passes through the Moren quarry, which contains sulfur rich siliceous rocks. No pyrite is found in the region. Bentonites are found in the distal facies, east of Sivridoğru Hill. This small bentonite deposit occurs at the Akıncı quarry but it is not economically viable (Fig. 2).

5. Fieldwork and analytical methods

Fieldwork included reconnaissance of the region and mapping at a scale of 1:25,000 (Fig. 2) using hand specimens as a basis for lithologic determinations and previously published local maps (Mutlu et al., 2005). Detailed mapping of the Düvertepe district at 1:10,000 scale, sampled both fresh and altered exposures at the various quarry sites and determined stratigraphic relationships.

Mineralogical and geochemical techniques are detailed by Ece and Schroeder (2007). Whole-rock chemical analyses were performed by ACME and ACTLABS Analytical Laboratories, Canada. Major and trace elements were analyzed using Spectro Ciros Vision ICP-OES for Ba, and Sc (0.2 g pulp sample by $LiBO_2$ fusion) and Mo, Cu, Pb, Zn, Ni, As (0.5 g sample leached with 3 ml of 2–2–2 $HCl–HNO_3–H_2O$ at 95 °C for one hour, diluted to 10 ml) and by Perkin-Elmer Elan 6100 ICP-MS for other elements. Differential thermogravimetric analysis (DTGA) was conducted at the University of Georgia, Athens (UGA) on a Hi-Res® TGA 2950 model instrument. Nitrogen was used as the purging gas. About 14 mg of sample powder was loaded in a platinum sample holder and then transferred onto a scale in the furnace. The chemical composition of the alunite samples was also examined in thin sections at the Istanbul Technical University (ITU) using a JEOL® JXA-8600 model superprobe with wavelength dispersive spectrometer (WDS) using a 15 kEV, 5 nA beam current and diameter of 10 μm. Mineral analyses and morphological and textural features of various clay minerals were carried out using a JEOL JSM-7000F model field emission scanning electron microscope (FE-SEM) (Bozzola and Russell, 1999) at ITU. A SPI-MODULE® sputter coater was used for Au–Pd alloy coating under operating conditions of 2 mbar, 15 mA and 50 s. This provided a ~150 Å coating thickness. Operating conditions of FE-SEM were 15 kV accelerating voltage, 5–15 mA current and 10–20 s counting time for each element.

Sulfur isotope studies of alunite at UGA include analysis of SO_2 which was produced via reactions of samples with V_2O_5, Cu metal and silica at 1050 °C. The $\delta^{34}S$ values are reported relative to Canon Diablo Troilite (CDT). Precision, determined by replicate analysis of laboratory standards, is better than $\pm 0.2‰$ (2σ). The $\delta^{18}O$ was measured via laser ablation using BrF_5. The δD was measured using Zn metal as a reductant. Isotope ratios were measured using a Finnigan MAT 252 mass spectrometer (S) or Finnigan MAT Delta E mass spectrometer (O and D).

The K–Ar age values were determined at Georgia State University using the method of Ece et al. (2008). Whole-rock samples were pulverized and chopped to fine size in a blender, to ensure equivalence of the respective portions taken for argon and potassium measurements. $^{40}Ar/^{39}Ar$ age determinations were carried out at the University of Michigan on a total of nine alunite samples using incremental heating method. X-ray diffraction analyses indicate that the mineral separates were composed largely of alunite minor to kaolinite and quartz. Alunite-rich cips measuring a few millimeters in diameter from this material were wrapped in pure Al foil and irradiated at the Mc-Master Nuclear Reactor at McMaster University in Hamilton, Ontario, and analyzed at the University of Michigan. All analytical data are reported at the confidence level of 1σ (standard deviation). Samples

were analyzed by the furnace step-heating method utilizing a double vacuum resistance furnace similar to the Staudacher et al.'s (1982) design. Details of the analytical methods and data treatment are given in Justet and Spell (2001) and Spell and McDougall (2003).

6. Results

6.1. Mineralogic, chemical and isotopic characterization of alteration products

X-ray diffraction studies reveal that kaolin-rich deposits consist essentially of kaolinite, quartz, and lesser amounts of alunite and opal-CT (IN-1 in Fig. 5). In contrast, alunite-rich deposits (e.g., in the Inüstü Hill area north of the Simav fault) consist of alunite, quartz, and halloysite. Mineral assemblages deeper in the Inustu Hill deposit are alunite-rich and shallower assemblages are richer in opal-CT. Hinckley's (1963) indices range from 0.4 to 1.2 (i.e., poorly- to well-ordered) with most of the kaolinites in the Düvertepe district composed of moderately-ordered varieties. Field-emission scanning electron microscopy (FE-SEM) shows that halloysite is only found in alunite nodules (Fig. 6A,B,C,D). Halloysite morphologies are seen as needle-like forms and fibrous tubes 2 to 3 μm in length. Outer diameters of the tubes range from 80 to 200 nm, and are formed on the edges of altered mica flakes. Kaolinite occurrences that originate from altered volcanics show growth stages on both feldspars and glass matrices and are very fine crystals (Fig. 6E). Euhedral pseudo-hexagonal book-shaped stacking sequences are common (Fig. 6E,F). Kaolinite stacking thicknesses range from 10 to 30 μm and finer microcrystalline quartz is often observed on the flakes. The occurrences of micro quartz crystals (Fig. 6G) and needle-like halloysite tubes (Fig. 6H) on the surfaces of alunite crystals are documented. The paragenetic sequence of mineralization is summarized into a schematic fashion which is shown in Fig. 7. Whole rock chemical analyses of the kaolins and alunite-rich samples are listed in ESM—Tables 1 and 2 (Electronic Supplementary Material), respectively.

DTA–TG study shows that kaolinite dehydroxylation begins at 500 °C and ends at around 700 °C, with a maximum water expulsion occurring in the range of 615 to 632 °C for the poorly- and well-ordered kaolin group minerals, respectively (Fig. 8). The endothermic peaks are slightly asymmetric to the low temperature side and measure about 13 wt.% loss in kaolinite-rich samples, which is very close to the ideal kaolinite value of 14 wt.%. Well-ordered kaolinites have broad endotherms, while more poorly-ordered halloysites have narrower endotherms. DTA–TG curves of the alunite-rich samples show a very minor initial ~80 °C peak, a second peak between 500 and 550 °C, and a third peak at 700–750 °C exhibiting alunite endothermic patterns typical to the mechanisms explained by Ece and Schroeder (2007).

Potassium–argon ages for alunite samples are listed in Table 3. The model ages of alunite mineralization range from 20.1 to 20.6 Ma in the south of graben, whereas, ages range from 17.3 to 19.2 Ma in the north of graben. One alunite sample shows a younger age as 15.3 Ma, which suggests that acidic hydrothermal activity continued

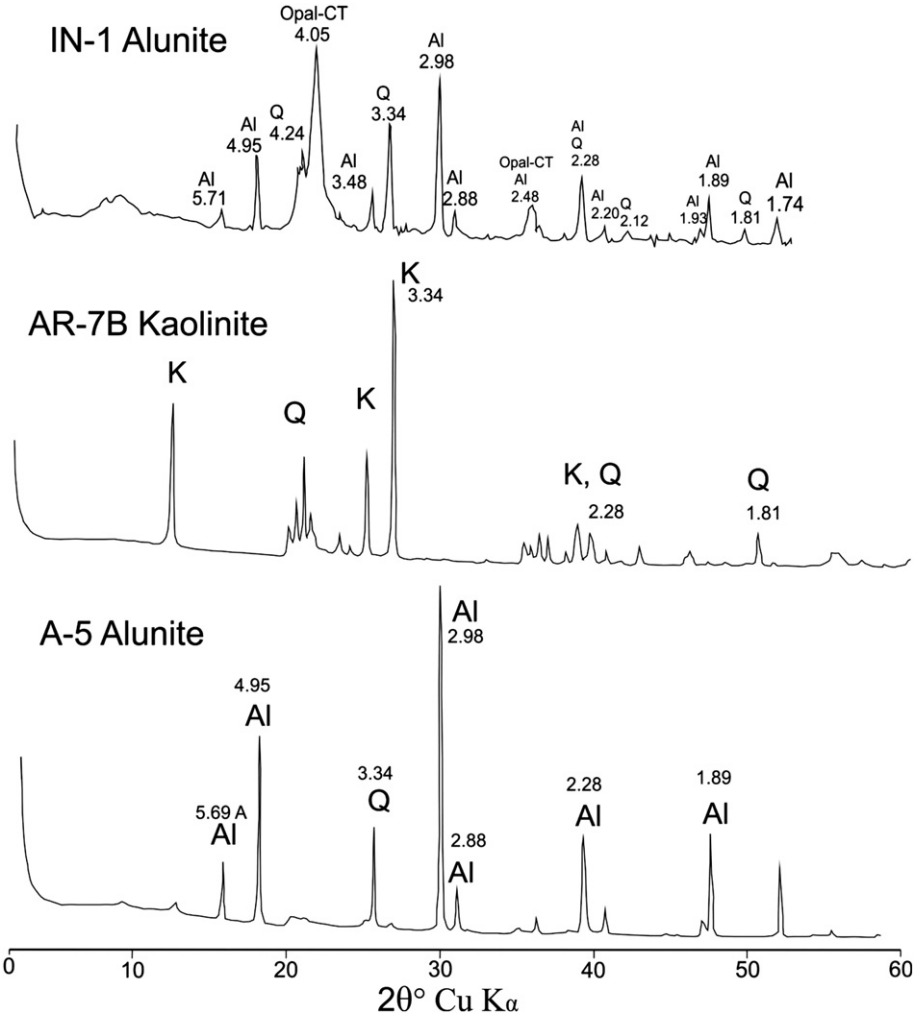

Fig. 5. The results of XRD studies on kaolinite and alunite samples. IN-1 and A-5 are from alunite cave in the Inüstü Hill, north of graben and AR-7B is from Arpatarla quarry, south of the graben.

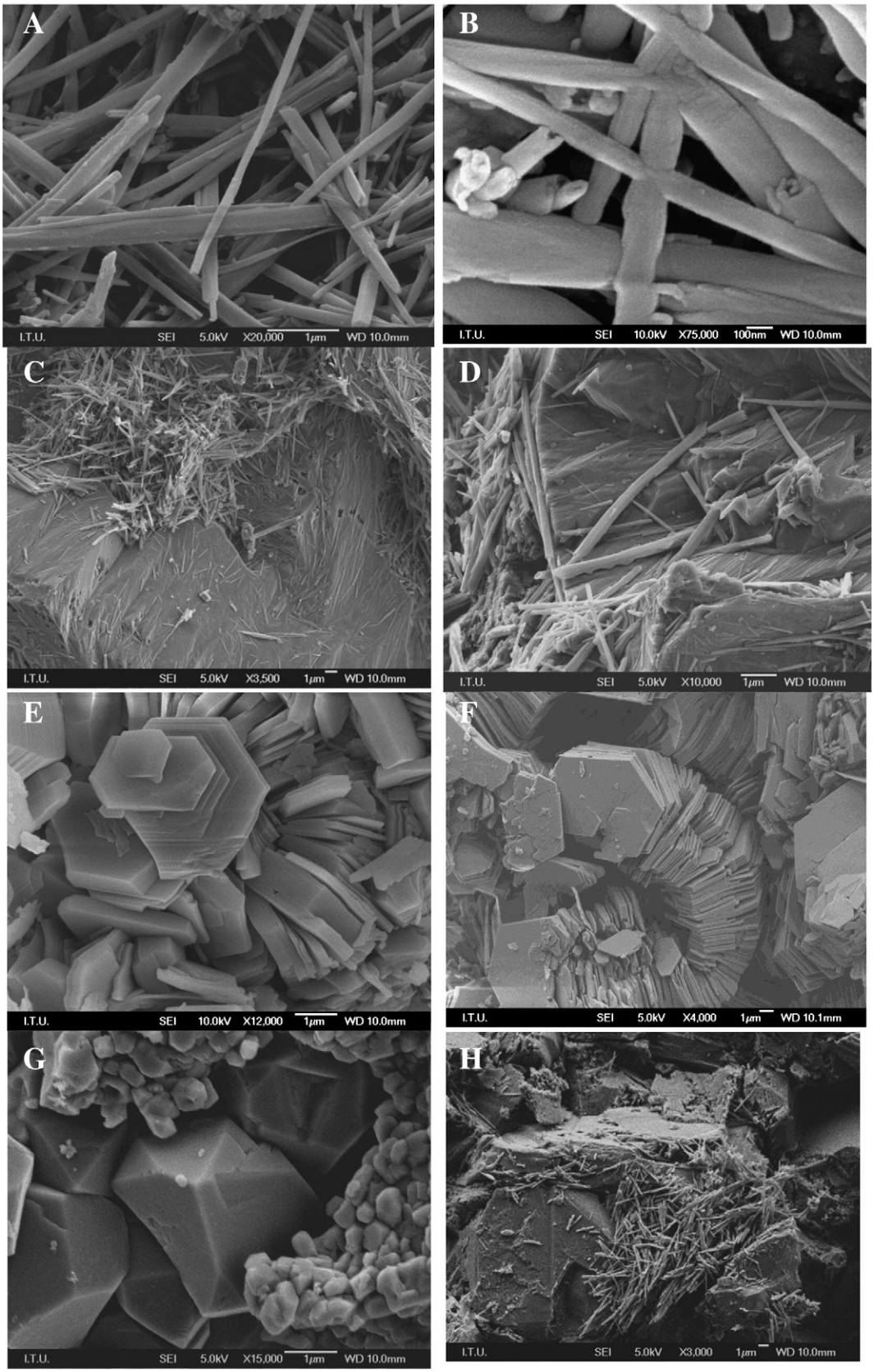

Fig. 6. FE-SEM photomicrograms of alunites and halloysites from Inüstü Hill; (A) irregularly distributed and intersection of many tubes shown as thin needle-shaped halloysite crystals; (B) show tubular structures of halloysite crystals in enlarged areas and show open-end tubular and onion-skin morphology; (C) and (D) show forming of needle-shaped halloysite crystals on altered feldspar grains; (E) vermiform–kaolinites (or book-shaped); (F) small well-formed hexagonal-shaped kaolinites are loosely packed; (G) nucleation of idiomorphic rhombohedral alunite crystals and occurrence of micro quartz crystals and (h) presents thin halloysite crystals forming on alunite surfaces.

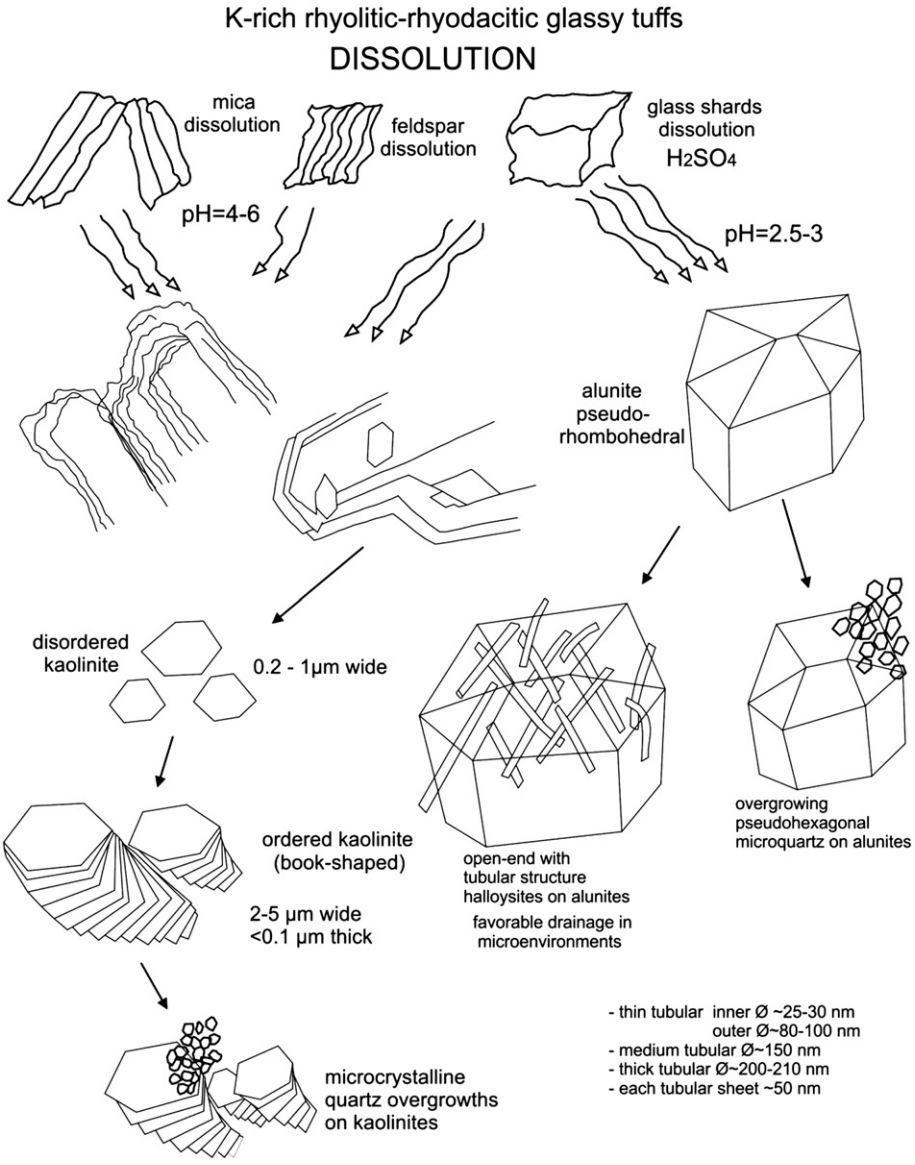

Fig. 7. The chart summaries paragenetic sequence of hydrothermal alteration and dissolution processes of rhyolitic–rhyodacitic tuffs and lavas to kaolinite and alunite, according to FE-SEM studies.

for a few million years on the north side of the graben after the major magmatic activities concluded. Apparent Ar/Ar ages of alunites range from 18.7 to 21.1 Ma in the south and 16 to 19.9 Ma in the north of graben. Ar/Ar dating results are also presented in Table 3. Ar–Ar plateau age determinations are presented in Fig. 9. Results indicate that the K–Ar dating method is compatible with the Ar–Ar method and by this approach, the overprinted geological events can be distinctly used to identify the timing of the influences of hydrothermal events.

Sulfur isotope studies revealed that the $\delta^{34}S$ values range from −1.55 to +6.18‰ for alunite (Table 1), indicating there is a little difference in the distribution of $\delta^{34}S$ values between north and south of the graben.

Hydrogen and oxygen isotopic compositions of the Düvertepe kaolinite samples are given in Table 2 and Fig. 10. They have δD values ranging from −49.0 to −94.3‰, concentrating between −75 and −90‰. The $\delta^{18}O$ values for kaolinite range from +5.8 to +17.1‰, with most values between +10 and +13‰. Using the Sheppard and Gilg's (1996) O isotopic fractionation factor between water and kaolinite in equation below,

$$1000\ln\alpha_{\text{kaolinite}-\text{water}} = 2.76 \times 10^6 \times T^{-2} - 6.75$$

and assuming the average Miocene meteoric waters was $\delta^{18}O = -4.5$‰ (we will discuss later) and water temperatures assumed to be in equilibrium at depth, calculated formation temperatures range from 38° to 129 °C (Table 2).

6.2. Kaolin chemistry

Chemical composition of kaolins and alunites from different quarries is listed in ESM—Tables 1 and 2 (Electronic Supplementary Material). The bulk sample wt.% ratios of the SiO_2/Al_2O_3 fall between 1.12 and 3.90, and it can be compared with other mineralogical compositions (ESM—Fig. 2; Electronic Supplementary Material). Based on wet chemical analysis, the high SiO_2/Al_2O_3 ratio obtained for the more compact kaolin is attributed to a large amount of very fine-grained quartz. These analyses confirm the presence of large amount of silica content in the samples (ESM—Table 1). Loss on ignition (LOI) for various kaolins varies between 8.5 and 13.9 with the upper limit, close to ideal kaolinite (13.96 wt.%). The triangular diagram (ESM—Fig. 2; Electronic Supplementary Material) with SiO_2, Al_2O_3 and $Fe_2O_3 + TiO_2 + MgO + Na_2O + K_2O$ values, shows that Düvertepe samples plot in an area of wide range of kaolin deposits similar to

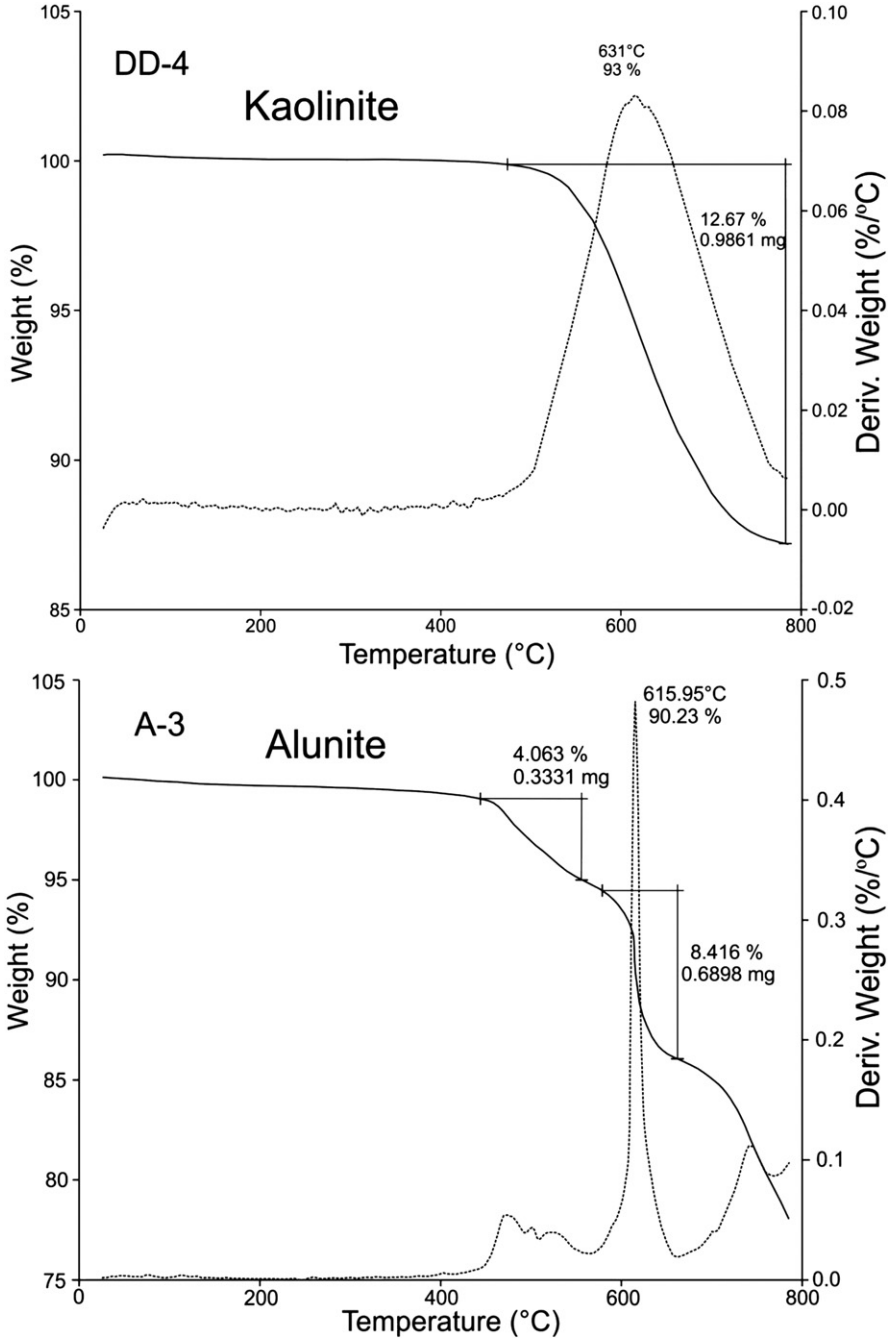

Fig. 8. The results of TGA studies on kaolinite and alunite samples.

those in Germany. The TiO_2 content varies from 2.5 to 7%, which is similar to sedimentary kaolin deposits (Schroeder and Shiflet, 2000). Strong depletion of alkaline and earth alkaline elements indicates that rhyolite–dacites and tuffs underwent intense leaching to form a high grade of kaolinization (ESM—Table 1; ESM—Fig. 2). Using the chemical index of alteration (CIA) = $[(Al_2O_3)/(Al_2O_3 + CaO + Na_2O + K_2O)] \times 100$ equation, the Düvertepe kaolinite has CIA values of 98.42–99.74 (Nesbitt and Young, 1982, 1984).

P_2O_5 wt.% values of the kaolins fall in the range of 0.07 to 0.3 and fresh volcanic rocks are in the range of 0.1 to 0.2. Sousa et al. (2007) reported that Ti–Nb–Ta–W–Zr elements are practically immobile in environments with high alteration grade. HREE and Y correspond to the relative zircon enrichment and loss of LREE during the leaching of phosphates. ESM—Fig. 3 shows the close linear relationship between Zr and TiO_2. Ti was used in the Nb versus Ta diagram (Fig. 11), which suggests a strong positive correlation of Ta and Nb enrichments in titanium oxides. A similar observation of positive correlation of Ta and Nb in Ti-oxide minerals was also reported by Sousa et al. (2007), who interpreted this relation between different kaolin facies suggesting that their origin was from the same sources.

6.3. Alteration paragenesis

6.3.1. Silicified bodies and silica sinter

Silicification affects pre-existing rocks but silica sinter is deposited from hot spring. Two broad and very thick silicified bodies are exposed along the fault zone in south of Arpatarla quarry (Fig. 2). One of these bodies is exposed further south in a quarry at Kabaağaçlı Hill, with approximately more than 50 m thick massive silicified rocks. The other was exposed in just south of Arpatarla quarry and the thickness varies

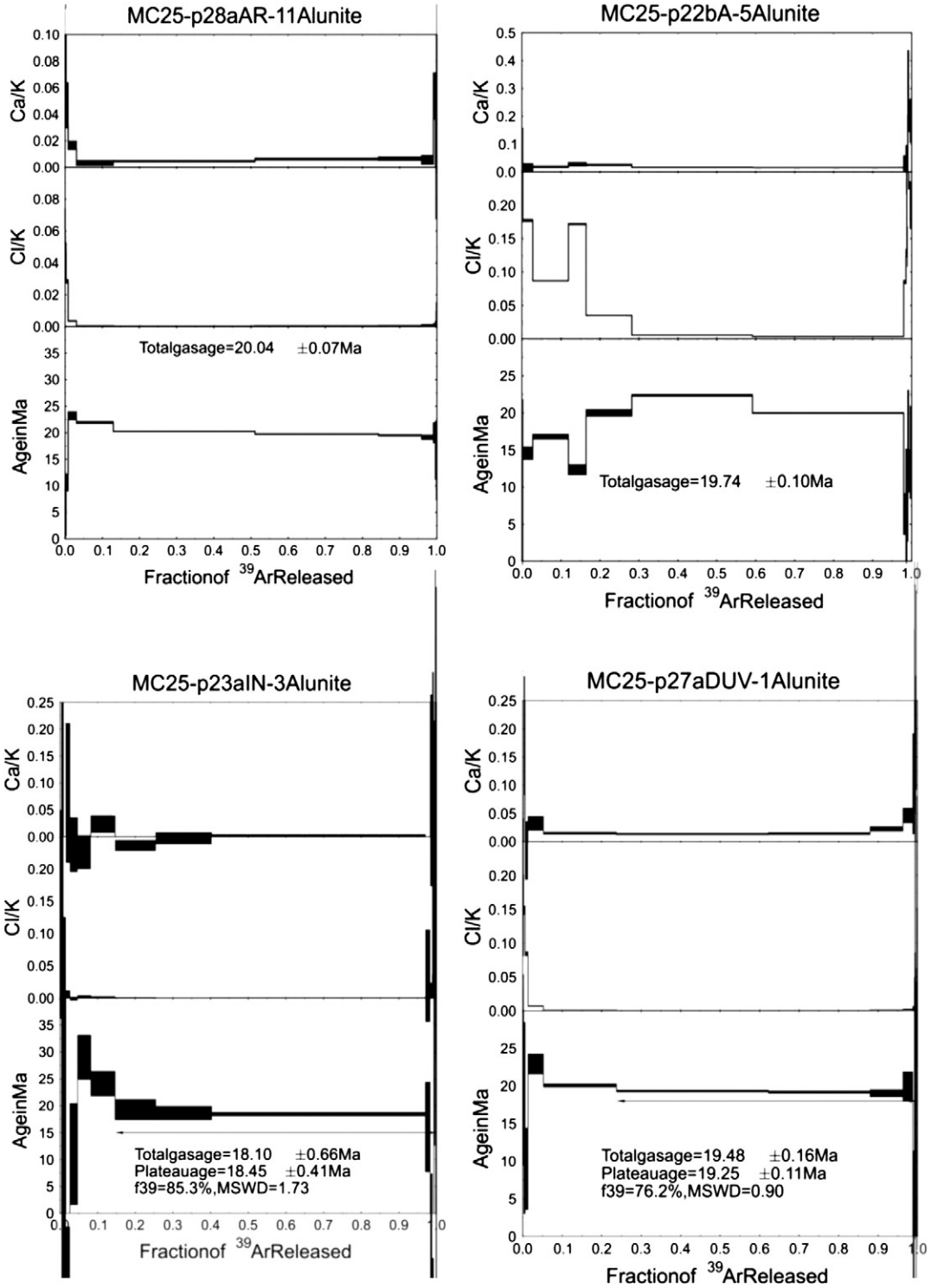

Fig. 9. Ar–Ar age dating, Ca/K and Cl/K spectra for alunite samples from the Düvertepe district. AR-11 and DUV-1 are from the Arpatarla quarry, south of graben and A-5 and IN-3 are from Inüstü Hill, north of graben. Cl/K and Ca/K values do not have error estimates and only their calculated values are shown. Errors in isochron diagrams are presented at 1σ level.

from 1 to 10 m at Arpatarlası Hill. The thick silicified rocks at Kabaağaçlı Hill is adjacent to rhyolites at south and therefore, giant volume of silica-rich hydrothermal fluids possibly derived from deep Si-leaching of ryholites and dacites at deep of the Simav Graben along the intersection of NW–SE trending fault with silicification destroying the primary rock texture. Silicified bodies above the kaolin deposits suggest the former presence of supergene ascending hydrothermal solutions. This process is evident in active and fossil geothermal systems worldwide where near-neutral pH alkali-chloride waters, oversaturated in silica, cool at or just below the ground surface (e.g., Fournier, 1985; Sillitoe, 1993; Herdianita et al., 2000). Similar silica-rich geothermal waters have been observed in Mexico (Keller and Hanson, 1968, 1969), Japan (Iwao, 1968) and Turkey (Sayın, 1984, 2007). When the ascending of saturated cation- and anion-rich (mostly silica- and sulfate-rich) hydrothermal solutions along fault zones gets close to the surface, pressure and temperature drop, pH increases close to neutral, spray over the volcanic

Table 1
Sulfur isotopic composition of alunite-rich samples.

Sample ID	Yield (mg)	Yield		K_2O (wt.%)	$\delta^{34}S$ (CDT)
		μmol	μmol/mg		
North of Graben					
Inüstü Alunite Cave					
A-1	25.72	145.0	5.6		1.53
A-2	23.72	73.9	3.1		2.02
A-3	22.22	95.0	4.3	8.68	1.86
A-4	22.23	109.4	4.9	8.87	3.07
A-5	23.63	38.4	1.6	8.31	−0.80
A-6	22.28	50.9	2.3		3.33
A-7	22.40	50.9	2.3		1.20
IN-1	23.36	68.2	2.9	4.50	2.06
IN-2	200.00	104.6	0.5	0.20	1.53
IN-3	22.00	38.4	1.7	2.85	2.54
IN-3	41.55	65.3	1.6	2.85	2.54
Düvertepe Quarry					
DUV-1	22.00	77.8	3.5	5.55	1.76
DUV-1A	26.07	101.8	3.9	5.55	1.85
South of Graben					
Arpatarla Quarry					
AR-11	25.40	26.9	1.1	3.69	1.25
AR-12	202.60	14.4	0.1		3.91
AR-13	203.20	9.6	0.0		3.88
AR-23	23.96	36.5	1.5	2.7	0.95
Sapçı Quarry					
S-1	202.30	403.2	2.0		3.20
S-2	22.16	37.4	1.7		6.18
S-5	22.19	95.0	4.3		0.08
S-7	23.48	37.4	1.6		5.76
S-10	22.63	49.0	2.2		−1.55
S-13	23.94	18.2	0.8		−1.10
S-14	22.76	58.6	2.6		−0.59
S-17	21.15	37.4	1.8		0.11
S-19	22.36	53.8	2.4		0.20
SAP-20	22.84	50.9	2.2	8.4	0.25

Table 2
O and D isotopic composition of kaolinite samples and calculated formation temperature, assuming $\delta^{18}O$ value of meteoric water is −4.5‰.

Kaolinite					
Sample ID	H2 yield (μmol/mg)	δD‰ (VSMOW)	δ180 ‰ (VSMOW)	Calculated formation temp. (°C)[a]	Average ısotopic temp. (°C)[a]
South of Graben					
Arpatarla Quarry					
DA-2	4.55	−49	10.5	82	
DA-3	4.61	−80.4	11.1	78	68
DA-4	2.75	−90.8	11.6	74	
DA-6	1.35	−81.9	17.1	38	
Cennet Cukuru Quarry					
CC-3	3.24	−82.9	14	57	
CC-8	3.29	−94.3	13.6	59	
CC-10	2.71	−69.4	15.5	48	55
CC-14	4.16	−80.8	13.6	59	
CC-15	4.2	−84.2	14.7	52	
Silica Sinter					
K-1	3.03	−82.5	10.9	79	81
SINTER			10.4	83	
Sapci Quarry					
SAP-1	4.45	−66	13.1	63	
SAP-3	4.82	−83.4	9.5	91	
SAP-4	6.55	−80	10.6	82	
SAP-9	4.01	−69.5	13	64	94
SAP-12	6.97	−80.5	6.4	122	
SAP-13	7.33	−77.9	6.4	122	
SAP-40	7.24	−82.1	7.3	112	
Arpatarla Quarry					
AR-9	6.88	−84.5	8.5	100	
AR-10	3.87	−67.8	14.8	52	
AR-15	6.09	−82.1	8.7	98	
AR-18	3.38	−70.3	13	64	
AR-22	2.55	−81.2	11.5	75	72
AR-26	2.22	−61.7	13.3	61	
AR-27	3.16	−89.3	12.6	66	
AR-28	3.9	−85.9	13.8	58	
North of Graben					
Doren Quarry					
DD-1	3.18	−77.3	9.2	94	
DD-3	1.97	−84.2	12.7	66	
DD-4	6.8	−81.3	5.8	129	
DD-5	5.82	−75.1	7.6	109	
DD-7	5.22	−74.7	9.6	90	
DD-8	4.38	−85	10.3	84	
DD-9	2.92	−93.5	8.9	96	89
DD-18	6.45	−79	9.8	88	
DD-20	3.39	−91	11.8	72	
DD-23	2.14	−88.5	12.8	65	
DD-40	3.92	−84.1	10.5	82	
DOREN			9.5	91	

[a] Sheppard and Gilg (1996).

tuffs, and consequently, dissolve supersaturated silica in the solution precipitated in those areas where they reached the surface forming the thick silica zones.

6.3.2. Siliceous veins

Siliceous veins occur in almost all hydrothermal kaolin deposits in different sizes in the Düvertepe kaolin district. Fe-oxide-rich horizons are the result of late-stage surface weathering. Due to lithological heterogeneous structure, opal and silicified layers are irregularly distributed. Observations in open quarries showed that silica veins are widespread and sulfur content also generally increases within siliceous veins. Hydrothermal silicification becomes more intense upward because cooling and dropping pressure of hydrothermal fluids facilitates silica precipitation in the upper part of upward fan-shaped faults and veins. Dill et al. (1997) pointed out that similar occurrence of hydrothermal silicification from ascending solutions in the western Peru kaolin deposit. These silica zones are the striking features of hypogene kaolin deposits in the Emet district (Sayın, 2007), which occurred ~60 km east of the Simav town. According to Hayashi (1973), α-quartz may be crystallized from the hydrothermal solutions at elevated temperature rather than opal. In the Otake geothermal area, Japan, quartz has crystallized above 100 °C, whereas opal was observed below 80 °C from the hydrothermal solutions (Hayashi, 1973). Kyle et al. (2007) reported from Uzon Caldera, Kamchatka, Russia that siliceous sinter (opaline spicules and opal-A is dominant phase) forming around spring at 83°–85 °C with pH of 5.9 and the visible association of microbial mats. We expect that silica sinter, which formed at the surface, must form at temperatures of <100 °C; more discussions about the age of opal have been done in later sections. All Düvertepe kaolin deposits contain significant amount of α-quartz, so it is possible to propose that hot acidic solutions may elevate the temperature of the medium in which amorphous silica (opal-CT) may have been recrystallized, or α-quartz has been formed from the solution directly (Keller and Hanson, 1968, 1969; Sayın, 2007). Quartz may be residual from the rhyolite parent rock and no beta-quartz was found.

6.3.3. Massive alunite–halloysite–opal-CT

Almost pure alunite mineralization is found close to the Inüstü Hill next to a small fault zone close to the main Simav Fault. These are mostly white to light yellow, hard, with granular texture and associated with thin silica zone. The occurrence of tabular-shape halloysite is only found during the SEM studies.

Pyrite mineralization was not observed in the kaolin deposits or parent rocks. However, mining operations found small amount of pyrite horizon in a core drilling at 15–20 m depth in only one kaolin quarry, located about 800 m south of Düvertepe, north of the graben. These samples were unfortunately not preserved. The sulfur content within

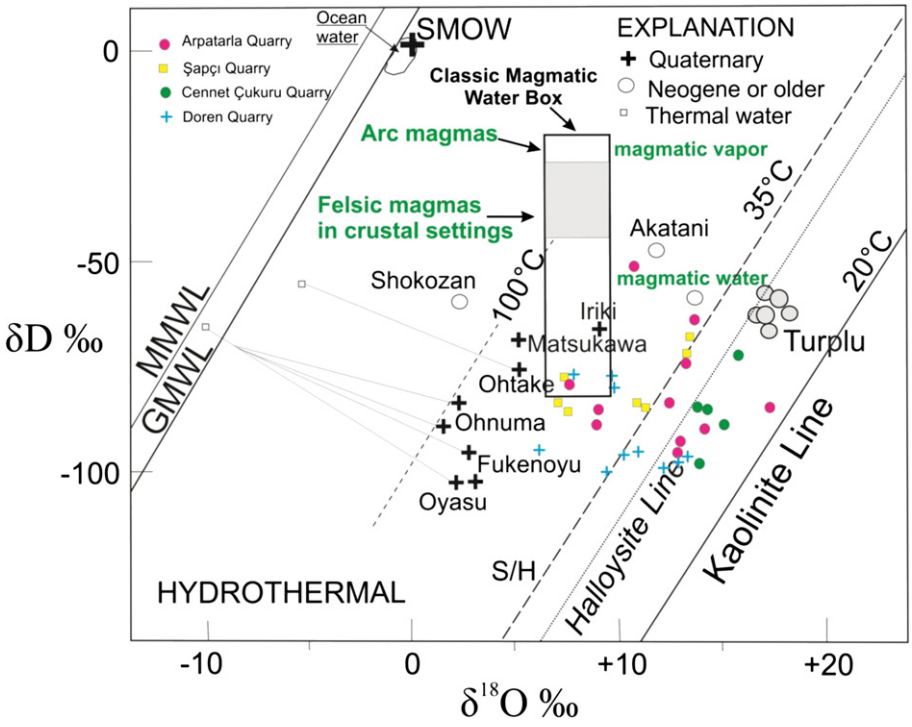

Fig. 10. The $\delta^{18}O$ and δD values of kaolinite from both sides of the graben, hydrothermal kaolinites from active geothermal fields and thermal waters near kaolinite locations in Japan (Hayba et al., 1985). The meteoric water line is $\delta D = 6.8\ \delta^{18}O + 10.5$ (Harris et al., 1999). The light dashed line shows the δD–$\delta^{18}O$ relation of kaolinite in equilibrium with meteoric water at 100 °C. Supergene versus hypogene lines are taken from Sheppard and Gilg (1996). Turplu halloysite values are from Ece et al. (2008). The line labeled S/H is equivalent to kaolinite in equilibrium with meteoric waters at temperatures of ~35 °C. MMWL: Mediterranean Meteoric Water Line ($\delta D = 8\delta^{18}O + 22$); (Gat and Carmi, 1970); GMWL: Global Meteoric Water Line ($\delta D = 8\delta^{18}O + 10$). Isotopic composition of magmatic waters from primarily andesite arc volcanoes and from felsic magmas floored by continental crust with the range of compositions ("boxes") classically considered for magmatic waters (Taylor, 1992).

the kaolin deposits varies depending on lateral and vertical distribution of alunite mineralization.

6.3.4. Kaolinite 1T–alunite–quartz

This mineral assemblage is commonly found in vein, veinlets and fault zones. Alteration of rhyolitic and rhyodacitic tuffs is more intense in silica and sulfur rich veins and is controlled by fracture systems. More alunite mineralization is found next to the fault zones where presumably large volumes of ascending sulfate-rich geothermal waters passed through these fault zones. Kaolin quarries provide very good exposures to examine epithermal zonations. No specific vertical zonation of the minerals has been observed, but both Fe-oxide rich and silicified layers are found at different levels. Alunite decreases in abundance laterally away from fracture systems. Some horizons also contain higher content of sulfur due to increased lateral permeability of tuffaceous materials. Alunite is intergrown with kaolinite and quartz and is mostly white to light yellow, relatively soft and has vuggy cavities. Geochemical analyses indicate that alunite samples are very poor in phosphate content (ESM—Table 2; Electronic Supplementary Material). Phosphate may have been scrubbled from the fluid owing to stepwise condensation and phase separation at depth (B.R. Berger, pers. comm.). These observations suggest that the source of sulfur and low phosphate content of the alunite may have a steam-heated or supergene origin (Rye et al., 1992; Ece et al., 2008). Vapors may be a predominant component of the ascending hydrothermal fluids and alunite formation because of low permeability and aquitard properties of volcanic and metamorphic basement rocks.

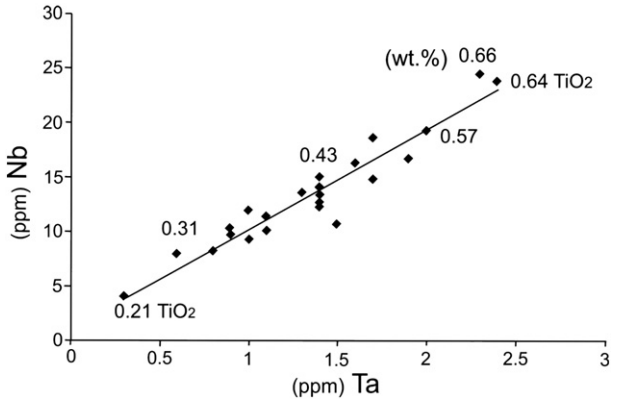

Fig. 11. Nb–Ta relation in kaolin samples shows positive correlation with increase of TiO_2.

6.3.5. Montmorillonite–kaolinite 1 Md–quartz

Montmorillonite is found in only one bentonite quarry, which is just north of Simav Graben, suggesting that smectite mineralization took place in the area where acidic hydrothermal fluids lost H^+ ions and became partially near to neutral fluids as they altered tuffaceous materials. Montmorillonite–quartz occurs in lateral horizon and is commonly associated with Fe-oxides and Fe hydroxides. The physical properties of bentonite samples are of not high quality for economic use.

7. Discussion

7.1. Mass transfer considerations

Mass transfer can be assessed by comparing chemical compositions of fresh and altered volcanic rocks (Gresens, 1967; Babcock, 1973; Grant, 1986; MacLean and Kranidiotis, 1987; Altaner et al., 2003). Warren et al. (2007) simplified the previously proposed equations by

substitution of Fv (volume factor: ratio of volume of the altered rock to the fresh rock) and canceling of density measurements, using the equation:

$$\Delta X = \left(\left(X^{Ai}/X^{Bi}\right)\cdot X^{B}\right) - X^{A}$$

where ΔX = mass change for mobile component X in g/100g or g/t, X^{Ai}/X^{Bi} = the ratio of the immobile element (Al is used in this study) concentration of the fresh rock to the altered rock, X^{B} = concentration of mobile component X in the altered rock, and X^{A} = concentration of mobile component X in the fresh rock. ΔX values of kaolins and alunites are listed in ESM—Tables 3 and 4 (Electronic Supplementary Material), respectively. Mass changes for mobile elements (ΔX) can be calculated from whole-rock geochemical data and evaluated graphically and related to associate hydrothermal alteration minerals using molar element ratios (Fig. 12).

Rhyolites and tuffs hosting quartz ± adularia ± alunite ± kaolinite ± smectite ± illite epithermal deposits undergo elemental mass changes associated with K-metasomatism, K–H-metasomatism and H-metasomatism (Warren et al., 2007). These metasomatisms are developed progressively upward and outward from the major fault zone and the site of mineralization depending on the chemistry of ascending hydrothermal fluid composition, temperature, volume of the fluid, complexity of fracture systems and chemistry and mineralogical compositions of siliceous volcanic rocks (Warren et al., 2007). The studies on mass transfer associated with alteration of volcanic rocks felsic composition in a subaerial hydrothermal system indicated that K-metasomatism is accompanied by silicification and dissolution of alkaline earth elements in deep leaching hydrothermal waters, which ascended through fault zones (Giggenbach, 1984, 1988). We observed that young fault systems within all kaolin deposits are filled with siliceous masses and some fault zones have rare amounts of oxidized pyrite as goethite.

Plots of (2Ca + Na + K)/Al versus K/Al molar ratios provide a graphical approach for evaluating the degree of K-metasomatism, K, Ca and Na depletion and SO_4-metasomatism affecting altered rocks (Fig. 12). The degree of K- and SO_4-metasomatisms can be determined from the slope of each line depending on the composition of parent rocks (Madeisky, 1996). HFSE's Ti, Zr, Nb, Y and Yb are relatively immobile during hydrothermal, diagenetic and weathering alteration, and during regional metamorphism up to mid-amphibolite facies (Maclean and Kranidiotis, 1987; Gifkins et al., 1995). Assuming Al as the most immobile major element during hydrothermal alteration, the magnitude of displacement from a parent rock varies compared to the original values of K, Na and Ca that were differentially leached out.

The gain of K and the loss of Na and Ca account for much of the mass transferred in shallow hydrothermal systems (Giggenbach, 1984, 1988). The degree of alteration, mass transfer and associated alteration minerals can be recognized using the (2Ca + Na + K)/Al versus K/Al molar ratio plot (Fig. 12). Fig. 12 shows that the chemical composition of parent rocks was ultrapotassic; therefore, $SO^{2-}{}_4$ input from geothermal waters was sufficient to form alunite after removal of silica from parent rocks. Highly altered rocks either accumulated close to kaolinite corner indicating maximum Ca, Na and K losses or showed a range of alteration on the pathway between kaolinite and alunite. The range of feldspar compositions and mixtures with biotite plots was in between 1.0 and 1.1. Fresh felsic rocks from Simav Graben area, as determined by their K/Al molar ratio, and fresh intermediate to mafic rocks plot progressively to the right of this line (Fig. 12) in proportion to the amounts of Ca content of total rocks (Warren et al., 2007). According to Fig. 12, studied fresh rocks are mostly high potassic siliceous rocks and concentrated between 1.0 and 2.0.

7.2. K–Ar and $^{40}Ar/^{39}Ar$ datings of alunites

The age of magmatism is about 19–21 Ma due to continuous extensional tectonism in the Simav Graben (Yılmaz et al., 2000). The results of K–Ar datings compare well with those of Ar/Ar datings on alunites. This study demonstrates that both methods produce very similar values. Very small differences in these two methods are related to the decay processes of radiometric potassium isotopes and analytical procedures. The K–Ar dating of alunite indicates that continuous hydrothermal activity likely occurred both in the north and in the south of Simav Graben. Based on Table 3, the north of graben alteration is 2–3 Ma younger than the south of the graben.

The agreement of K–Ar dating method is quite good with the $^{40}Ar/^{39}Ar$ plateau ages on alunite associated with the kaolin mineralization (Fig. 9). Plateau ages between 18.73 ± 0.16 and 21.10 ± 0.18 Ma in the south of the graben and 18.06 ± 2.68 and 19.87 ± 0.20 Ma in the north of the graben suggesting that most of the kaolin deposits formed over a period of few million years.

According to Ar/Ar ages, statistical deviations for total gas ages range from ±0.07 to 0.18 Ma in the south and ±0.1 to 2.68 Ma in the north, and for plateau ages ±0.11–0.16 Ma and ±0.3–0.41 Ma, respectively (Table 3). This reflects the closure of Ar diffusion in

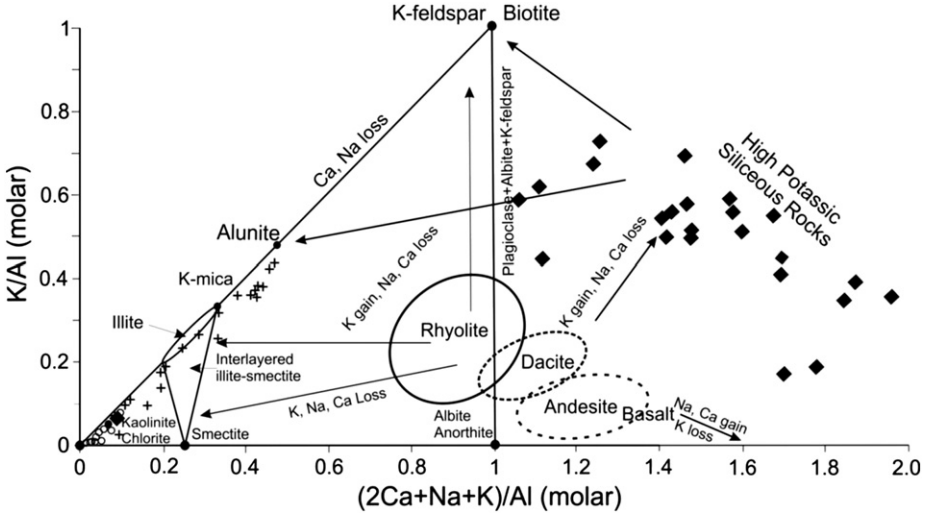

Fig. 12. Molar element ratio of (2Ca + Na + K)/Al vs. K/Al for typical fresh volcanic rocks (Warren et al., 2007). Mass transfer processes are shown with arrows that vector toward associated alteration minerals. Compositions of fresh volcanic rocks are from the Düvertepe District (Çoban et al., 2012). "o" symbol designates kaolin and "+" symbol designates alunite samples (data are from EDS—Tables 1 and 2) (Electronic Supplementary Material).

Table 3
The comparison of the results of K–Ar and Ar–Ar dating of alunite samples.

K–Ar								Ar–Ar	
Material	Test portion mass (mg)	Mass lost during extraction (dag/kg)	Mass fraction potassium (as K) (dag/kg)	Mass fraction potassium (as K_2O) (dag/kg)	Radiogenic argon (%)	Radiogenic argon (nmol/kg)	Apparent age (Ma)	Apparent age (Ma) Total gas age	Apparent age (Ma) Plateau age
South of Graben									
AR-23	122.1		2.04 ± 0.02	2.45 ± 0.02	88	73 ± 2	**20.6 ± 0.5**		
SAP-20	566.1	3.9	2030 ± 0.02	2.77 ± 0.03	95	82 ± 2	**20.4 ± 0.6**	**21.10 ± 0.18**	
AR-11	691.0	9.9	1.44 ± 0.01	1.73 ± 0.02	92.2	51 ± 1	**20.4 ± 0.6**	**20.04 ± 0.07**	**19.79 ± 0.16**
AR-11 (rep)	111.1		1.30 ± 0.01	1.57 ± 0.02	88	46 ± 1	**20.1 ± 0.5**		
AR-29								**18.73 ± 0.16**	
DUV-1								**19.48 ± 0.16**	**19.25 ± 0.11**
North of Graben									
IN-3	489.4	7.9	2.38 ± 0.02	2.87 ± 0.03	14.40	76 ± 9	**18.2 ± 2.2**	**18.10 ± 0.66**	**18.45 ± 0.41**
A-3	737.0	16.30	6.96 ± 0.07	8.39 ± 0.08	95	210 ± 5	**17.3 ± 0.5**	**15.98 ± 0.32**	**19.07 ± 0.30**
A-4	738.0	16.7	7.74 ± 0.08	9.33 ± 0.09	97.6	259 ± 6	**19.2 ± 0.5**	**19.87 ± 0.20**	
A-4 (rep)	106.0		7.21 ± 0.07	8.69 ± 0.09	94	238 ± 6	**18.9 ± 0.5**		
A-5	122.6		7.86 ± 0.08	9.47 ± 0.09	94	262 ± 6	**19.1 ± 0.5**	**19.74 ± 0.1**	
IN-1	116.1		3.34 ± 0.03	4.03 ± 0.04	35	89 ± 5	**15.3 ± 0.8**		
IN-2								**18.06 ± 2.68**	

different alunite samples during the continuation of thermal evolution of Düvertepe district and Simav Graben. Statistical deviation intervals suggest that hydrothermal activity, which reflects the isotopic closure temperatures of alunites, continues in a longer period in the north than in the south. The blocking temperature for alunites is estimated to be ~300 °C or less, even for a fast cooling rate of about 100 °C/Ma, which would be typical of epithermal environments (Arribas et al., 2011). Subsequent geological evolution of Simav Graben via fossil and active hot springs might have played an important role in the formation and resetting of isotopic closure ages of alunites.

The present day geometry of Düvertepe kaolin district looks like a broad angle-shaped valley 9–10 km wide, with southern hill elevations ~1250 m, northern hills ~950 m, and the lowest level at ~350 m. The elevation of alunite cave at Inüstü Hill within the north confines of the graben is ~550 m and it is exposed on the surface. The combination of field observations and estimated closure temperature of alunite mineralization leads us to conclude that alunite mineralization took place much deeper than on present day depth. For this reason, alunites formed at ~300 °C or less and significant volumes of rocks have eroded since Early Miocene.

7.3. Sulfur isotope composition of alunites

The alunite samples collected from the various kaolin quarries in both sides of the graben show little difference in the distribution of $\delta^{34}S$ values. The depleted $\delta^{34}S$ values of alunite strongly suggest that local meteoric water of higher pH had partially mixed with a magmatic dominant fluid during the initial stage of fossil hydrothermal activities. The $\delta^{34}S \approx 0‰$ composition of the alunite suggests that the source of the sulfate had an isotopic composition of bulk magmatic sulfur (Rye et al., 1992). The source could have been SO_2 or H_2S that was oxidized by interaction with groundwater or the atmosphere, but the minimal fractionation suggests that SO_2 was the dominant sulfur species (Love et al., 1998). Rye et al. (1992) argue that in magmatic hydrothermal systems the isotopically depleted sulfur ($\delta^{34}S \approx 0‰$) in sulfides is derived from H_2S whereas the isotopically enriched sulfur ($\delta^{34}S \geq 10‰$) in alunite is derived from H_2SO_4. They proposed that alunite in the steam-heated environments forms through oxidation of H_2S with a near-zero $\delta^{34}S$. These results are similar to the data presented in Table 1. Love et al. (1998) also argue that the alunite formed in a steam-heated environment from the oxidation of H_2S expelled from an underlying boiling hydrothermal fluid; its $\delta^{34}S$ composition is too low for a normal magmatic hydrothermal SO_2 sulfur isotope signature produced by fractionation of a small amount of SO_2 from a predominantly H_2S-bearing magma (Rye et al., 1992). The SO_2-rich fluid from which the alunite formed must have had a sulfur isotope composition similar to that of the magma. This model is matching with Simav Graben system because Simav River flows inside the graben and meteoric waters topographically infiltrate down from horst to deep sources.

Paleo-hydrology features of the Düvertepe district are similar to those of Simav Graben, using horst structure, Miocene sediments and Simav metamorphics as recharge areas. Alunite mineralizations were concentrated along some fault zones in the upflow area of hydrothermal fluids in north of the graben where high sulfur fugacity was likely dominant. The slightly positive $\delta^{34}S$ values of those alunites suggest that the sulfur-bearing fluids during the early stage of hydrothermal activity had acidic pH and low fO_2 (Ohmoto, 1972). Geothermal waters strongly indicate that the fO_2 was adequately high to maintain SO_4^{2-} as the dominant sulfur species relative to $H_2S_{(aq)}$ during alunite deposition. The removal of enormous quantity of oxidized H_2S from the fluid phase ($SO_4^{2-}{}_{(aq)}$) likely further increased the SO_4^{2-} to $H_2S_{(aq)}$ ratio in the fluids (Ohmoto and Rye, 1979). SO_2 gas disproportionates to H_2S and H_2SO_4 below 400 °C in the presence of water by the following reactions (Holland, 1965, 1967; Sakai & Matsubaya, 1977): $SO_2 + H_2O = H_2SO_3^{2-}$ and $4H_2SO_3^{2-} = 3H_2SO_4 + H_2S$, depending on sulfur redox conditions. Using this approach, the interaction of the sulfuric acid solutions with the rhyolitic–dacitic tuffs may explain the origin of kaolinite and alteration zones. It is possible to suggest that sulfur originated by either partial melting which produced magmatic solutions or dissolution or leaching of pre-existed sulfate-bearing magmatic sources (Ohmoto and Rye, 1979). Later, steam-heated SO_2-rich solutions migrated upward through fracture systems. All positive $\delta^{34}S$ values are consistent with deep magmatic sulfur sources.

7.4. Hydrogen and oxygen isotope composition

During the Early Miocene, the Mediterranean Sea and the Indian Ocean were connected to each other, Neo-Tethys Ocean was open between Anatolian landmass and Arabian Platform, and Turkey was located about 250 km south of the present geographic location (Görür and Tüysüz, 2001; Hüsing et al., 2009). Highlands were dissected in the Aegean region by fault-bounded grabens of various sizes and orientations; the Aegean Sea probably did not exist and its present site was occupied by highlands. As a result of paleogeographic and paleoclimatic evolutions, moisture carrying dominant and southerly warm supreme trade winds was coming to the Aegean Region from the Neo-Tethys Ocean. Consequently, $\delta^{18}O$ composition of meteoric waters during Early Miocene was different from the present day's values ($\delta^{18}O = -7/-8‰$) and they were much enriched. For this

reason, we assume that Miocene meteoric water values were similar to the present day's values, $\delta^{18}O = -4.5‰$, for the Simav region that was located in the present day latitude of the Mediterranean Coast of Turkey during Early Miocene.

Stable isotope δD and $\delta^{18}O$ compositions of kaolinites from fossil Düvertepe hydrothermal fields can be compared to other groups of kaolinites from active hydrothermal fields such as those in Japan (Fig. 10). Water temperatures, assumed to be in equilibrium at depth, have been calculated considering a $\delta^{18}O = -4.5‰$ for Miocene meteoric water (see the above discussion) and using the fractionation factor equation of Sheppard and Gilg (1996), ranging from 38 °C to 129 °C (Table 2). As mentioned earlier, a significant volume of rocks has been eroded since Early Miocene and kaolin deposits originally formed in much deeper environments. Model temperatures do not show significant difference between north and south of the graben (Table 2). The isotope data for the Düvertepe kaolinites are more enriched than the primary magmatic H_2O, indicating that the Düvertepe kaolin district samples developed under hydrothermal alteration conditions with subsequent evaporative modification, resulting in relative enrichment of heavy isotopes (Taylor, 1979; Sheppard and Gilg, 1996; Gilg et al., 2003). By comparison, Hayba et al. (1985) documented that the isotopic composition of kaolinites formed in a steam-heated environment from active Japanese hot springs plot very close to the line, which marks kaolinites that would be in equilibrium with meteoric waters at 100 °C.

The kaolinite line corresponds to equilibrium with meteoric waters at 20 °C (calculated using the fractionation equations of Sheppard and Gilg, 1996) and the S/H line is equivalent to kaolinite in equilibrium with meteoric waters at temperatures of ~35 °C. The formation of clay deposits occurred during the late stage mineralization period and consequently isotopic equilibrium was established at relatively low temperatures compared to the deep reservoir, resulting in kaolinite relatively enriched in ^{18}O. This enrichment in $\delta^{18}O$ explains why the values of kaolinites from fossil geothermal fields are shifted to the kaolinite line, whereas δD and $\delta^{18}O$ compositions of kaolinites from the current active geothermal fields of Japan are close to 100 °C kaolinite line (Fig. 10). For comparison, isotopic composition of whole rock, feldspar and quartz samples from hydrothermal deposits of the Marysvale volcanic field in Utah revealed that $\delta^{18}O$ values range from 0.2 to 4.7‰ for whole rock from −3.7 to −7.5‰ for feldspar phenocrysts and 1.5–11.4‰ for quartz as a function of depth (Cunningham et al., 1998). The oxygen becomes systematically heavier due to ^{18}O enrichment relative to ^{16}O toward the surface. The interaction of meteoric water with $\delta^{18}O$-enriched feldspar-, hornblende- and volcanic glass-rich volcanic rocks under deep hydrothermal circulation resulted in enrichment of the geothermal water composition compared to the meteoric water (Uysal et al., 2000, 2006). Similar observations are seen for the δO^{18} values of hydrothermal silica minerals and in-situ temperature measurements in Yellowstone, USA (Sturchio et al., 1990). The variability of $\delta^{18}O$ and δD values changes as a function of temperature that led to a large degree of fractionation between liquid and vapor (Faure, 1986). Thus, Düvertepe kaolinite samples formed under higher water reaction temperatures (e.g., >170 °C) would have relatively constant $\delta^{18}O$ and δD isotopic compositions (Table 2). The distribution of $\delta^{18}O$ and δD compositions of various Düvertepe kaolinite samples shows wide distribution pattern (Fig. 10) suggesting lower and variable temperatures at the time of crystal growth.

In addition to magmatic waters, it is well-known that local meteoric waters are the major source of fluid in continental geothermal systems. The fractionation of hydrogen isotopes between water and hydrous rhyolite magma varies primarily on water content and is therefore, dominantly controlled by temperature and minor pressure dependent (Taylor, 1992). Variations in δD of kaolin minerals in the Düvertepe Kaolin district (Fig. 10) indicate mixing with different meteoric waters rather than variations in the δD of magmatic water. Periods of closed-system degassing were punctuated by eruption and open-system behavior, as evidenced by the different ages of alunite mineralization along the north and south sides of the graben (~18 Ma and ~20 Ma, respectively). By analog with step-wise closed-system degassing processes in other magma systems, magmatic water may have been added to a hydrothermal system upon pressure-equilibration of rhyolitic magma in the Düvertepe district.

7.5. Supergene versus hypogene kaolinization

The distinction between hypogene and supergene kaolinization has been made using various element ratios in kaolin (e.g., P versus S, Zr versus Ti, Cr + Nb versus Ti + Fe and Ce + Y + La versus Ba + Sr) (Dill et al., 1997). There are compositional similarities in both andesitic volcanism and basin and range extension tectonism between Western Turkey and Central Volcanic Zone of Andes, which allows for comparison of alteration indices for the two systems. Dill et al. (1997) demonstrated that S, Ba, and Sr are considerably enriched in kaolin during hydrothermal alteration, whereas Cr, Nb, Ti, and lanthanides are concentrated mainly during weathering. Both P_2O_5 and SO_3 are enriched under the influence of hydrothermal alteration in hypogene kaolin deposits by the presence of alunite and some aluminum–phosphate–sulfate minerals. The enrichment in P_2O_5 content in kaolin depends on the basement rock types and mineral assemblages through which geothermal waters passed. It was proposed that the P_2O_5 content rises with degree of supergene alteration (Dill et al., 1997), but Rye et al. (1992) proposed that high P_2O_5 content is related to the deep source for hypogene origin. Earlier findings of Ece and Schroeder (2007) studying halloysite–alunite deposits in Northwest Turkey support the latter.

Zr is widely accepted as very immobile under weathering conditions. Ti is mostly concentrated in sedimentary kaolin deposits (Schroeder and Shiflet, 2000; Ece and Nakagawa, 2003; Railsback, 2003) and also in the form of anatase by hydrothermal fluids (Yau et al., 1987). Distinction studies on supergene versus hypogene origin of kaolin deposits from the Central Andes of Peru showed that supergene kaolins are more enriched in Zr and TiO_2 than hypogene kaolins (Dill et al., 1997). These geochemical indices are highly dependent on the conditions of chemistry, temperature and acidity of geothermal waters and composition of magmatic rocks passing through inside. Zr is partially mobile in hydrothermal fluids at low pressure (<2 kbar), low temperature (<500 °C) and high water/rock ratios. Köster (1974) discussed Cr^{3+} substitution with Ti^{4+} in TiO_2 modifications and with Fe^{3+} in FeOOH during supergene kaolinization. Nb and Ti have similar ionic radii and their substitution in TiO_2 is expected in supergene alteration. Dill et al. (1997) showed that pure supergene kaolin deposits contain high Cr and Nb (~100 ppm), whereas these elements are usually very low (7–80 ppm) in hypogene deposits because they are extremely insoluble near ambient temperature. Düvertepe kaolins contain the coupled elements (Cr + Nb) about 8–50 ppm which suggests hypogene origin (Fig. 13). Cr presents as soluble species at pH<4, hydrothermal kaolin deposits in which alunite coexists with kaolinite require pH<4 and this kind of acidic solutions is very typical of hypogene environments (Dill et al., 1997). This phenomenon better explains Cr + Nb enrichment in supergene environments. Also, at pH<4, Ti and Fe can be dissolved and are removed from the system; therefore, Ti + Fe content is low in hypogene environments. Düvertepe samples fit in the range of hypogene environments in Fig. 13.

Ba and Sr can substitute for each other and often occur at elevated levels in hypogene deposits. Light REEs are considerably enriched in supergene kaolinization (Maksimovic and Panto, 1983; Dill et al., 1997). This is expected due to solubility behavior of LREEs under hot and acidic conditions. There is clear evidence for an age difference between north and south of the graben. Also alunite mineralization is concentrated in the north and less intense and spread out in the south. Supergene–hypogene distinction can be made based on these independent indices. Fig. 13 suggests that Düvertepe kaolins are

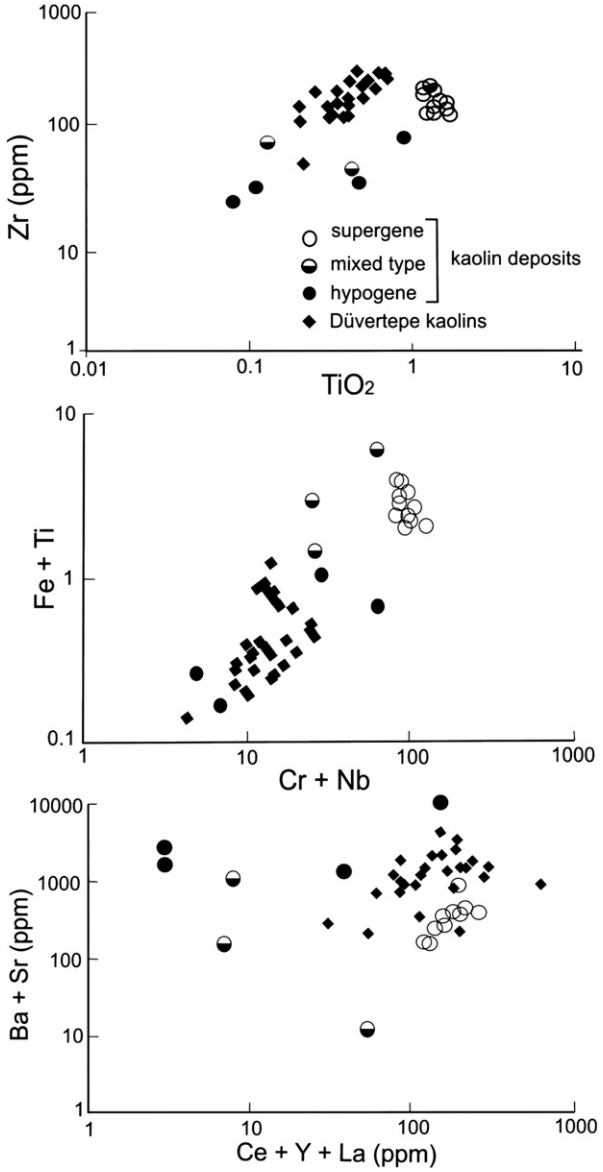

Fig. 13. Zr vs. TiO_2, Fe + Ti vs. Cr + Nb and Ba + Sr vs. Ce + Y + La plots of kaolinite samples from various quarries both sides of the graben. Solid symbols represent hypogene, supergene and mixed-type origins of kaolin deposits in Peru (Dill et al., 1997).

between supergene and hypogene alteration fields with an influence of supergene overprint after hypogene alteration. Direct comparison between the Simav and Peruvian data sets is partially limited by differences in host rocks and the absence of copper oxide minerals at Simav (Dill et al., 1997).

8. Proposed hydrothermal alteration model

The zonal patterns are characterized by a sequential appearance of clay minerals with increasing temperature. Halloysite, kaolinite and pyrophyllite are associated with the stable silica polymorph quartz formed at low pH and silica saturated conditions (ESM—Table 5; Electronic Supplementary Material). The high permeability of adjacent rocks is vitally important for the occurrence of the formation of halloysite and exportation of dissolved silica (Ece et al., 2008). Halloysite often forms next to or underlying limestone formations where pH is raised, relative to where kaolinite forms in the underlying volcanic environments (i.e., reactants are more slowly removed).

The component Al_2O_3 is often assumed as immobile during hydrothermal alteration because of its low solubility in moderately acid solution. If the solution pH is less than 4 at high temperatures then Al_2O_3 is mobile and SiO_2 is relatively insoluble (Inoue, 1995). Field studies show that fault zones within kaolin bodies are rich in silica, iron, and sulfate. The porous silica zones occur in the central portion of the deposit, which corresponds to a vent of ascending geothermal waters (Inoue, 1995), which is observed in almost all Düvertepe kaolin deposits. Fault zones also contain high sulfur content but distally kaolinization decreases as hydrogen ions are consumed by hydrolysis reactions with silicates. When the ascending geothermal waters rise through both fault zones and rhyolite–dacites and decreasing temperature, K-feldspars alter to alunite at very low pH (~2). With continuous reaction, pH gradually increases (~4) and K-feldspars alter to kaolinite.

The presence of muscovite-rich dacites at the Arpatarla quarry (south of Simav Graben) results in a sequence of K-feldspar → muscovite → kaolinite as a function of decreasing temperature, $[K^+]/[H^+]$ ratio, and pH. Kocataş Hill contains centimeter muscovite flakes in a quartz dacite intrusion and suggests that they have undergone the influence of hydrothermal alteration. Reactions never reached a full argillic alteration stage. The occurrence of bentonite deposit to the east of Sivridoğru Hill, north of Simav Graben, further suggests a distal decrease in acidity and temperature of geothermal waters.

During low-sulfidation events (i.e., adularia–sericite type hydrothermal systems analogous of submarine massive sulfides), Na, K, Ca and relatively smaller amounts of Si are dissolved and leached away from kaolin body. Volcanic blocks (15–30 cm) and surrounding tuffs observed in the field are partly kaolinized during hydrothermal alteration. Quartz is the main vein mineral where hydrothermal breccias are commonly found in many kaolin deposits occurring on both sides of the vein that are up to 2–5 m of the vein width. These breccias comprise subangular to subround clasts of previously altered host rocks. The matrix is made up of cryptocrystalline, crustiform, and colloform banded quartz attributed to hydrothermally driven diffusion and soft sediment deformation, adularia, and sulfide minerals and altered K-feldspar.

During high-sulfidation events (i.e., alunite–kaolinite or acid-sulfate type hydrothermal systems), geothermal waters at high temperature and pressure are supersaturated with K^+ and $SO^{2-}{}_4$. All high sulfidation activity along the Simav Graben is concentrated in the Düvertepe and Şaphane districts (Fig. 1) and all low sulfidation occurrences are mostly in the central part of the graben. Based on tectonic and magmatic evolution history of the Aegean region, we suggest that low sulfidation metal epithermal mineralizations occurred later than kaolinite mineralization. Leaching of Si from tuffs, oxidation from shallow groundwaters causes enrichment in Al_2O_3 content, thus forming alunite in the ranges of 210°–490 °C (Xiangji and Fusheng, 1998). A high-temperature acid solution at depth has more capacity than surface solutions to leach rock-forming elements regardless of the different parent rock types. These very aggressive solutions produce kaolin minerals, pyrophyllite and silica minerals. Native sulfur, pyrite and alunite are major constituent minerals characteristic of this type of alteration (Inoue, 1995), although the former two phases are rare in the Düvertepe and Şaphane districts. Silica solubility decreases with decreasing pH and dissolving of SO_2 will produce H_2SO_4 in boiling water, which causes precipitation of alunite at pH 2–2.5 in near-surface conditions (Browne and Ellis, 1970; Simmons and Browne, 2000). Quartz solubility also decreases as temperature decreases (Fournier, 1985), such that low-grade alunite precipitation accompanies silica deposition along fault zones.

The high-sulfidization style is observed in almost all kaolin deposits and veinlets in the Düvertepe district. The main fault zone in the south of Şapçı–Arpatarla quarries extends in NW–SE direction indicating that ascending hydrothermal fluids brought up Si-rich waters, which cooled to precipitate more than 10 m thick silica sinter masses along the fault zone in Arpatarlası Hill. More than 50 m thick massive silicic rocks are exposed as the result of vertical displacement in the

north of WNW–ESE trending fault zone in Kabaağaçlı Hill (south of the study area). The presence of large alunite mineralization in Inüstü Hill implies that sulfate input is coming through geothermal waters along fault systems. There is no field evidence to support the concept that acidic fluids originated by descending along fracture zones and forming alunite.

The frequent association of alunite and kaolinite is expected on the basis of phase equilibrium data for both hot spring and higher temperature environments (Hemley et al., 1969). Hemley et al. (1969) emphasize that rather high acidity is implied from their experiments of silicate–alunite systems at the elevated temperatures. Field studies revealed that major kaolin deposits in south of the graben are close to a rhyolite intrusion, which was one of the major heat sources in the area (Fig. 14). Pyrophyllite is predicted at temperatures from 270 °C to 340 °C, at a pressure of 100 MPa and quartz saturation, whereas kaolinite replaces pyrophyllite at temperatures below 270 °C (Hemley et al., 1980). First order genetic classification of epithermal deposits and the comparison of low-sulfidation versus high-sulfidation, based on alteration and mineral assemblages are summarized in ESM—Table 6 (Electronic Supplementary Material).

Under high-sulfidation conditions at depths ~3 km, intense leaching and alteration result from magmatic origin acidic solutions derived from magmatic vapor (Stoffregen, 1987; Vennemann et al., 1993; Hedenquist et al., 1994; Stoffregen et al., 1994; Arribas, 1995; Wang et al., 1999; Sillitoe and Hedenquist, 2003; Chouinard et al., 2005; Wang, 2010), where these studies indicate the abundance of vapor-rich inclusions in quartz samples and alteration mineral assemblages with homogenization temperatures ranging from ~150 °C up to 500 °C. The abundance of vapor-rich inclusions in advanced argillic alteration zones confirms vapor-rich environment and a wide range of temperature gradients during the formation of alunite and silica (Stoffregen, 1987; Hedenquist et al., 1994; Wang, 2010). Fluid inclusion measurements in alunite–silica alteration zones suggest that alunite itself is stable up to at least 450 °C (Stoffregen, 1987). Thermodynamics data (Hemley et al., 1969, 1980) also suggest that when strongly acidic solutions react with volcanic tuffs and rocks, it results in high silica activity in the liquid phase (Fournier, 1985; Africano et al., 2002). The silica activity–temperature relations of metastable polymorphs of silica precipitating together with alunite or with kaolinite at 250 bar are well documented (Fig. 2 in Henley and Berger, 2011). During the cooling process, metastable silica transitions through a sequence of polymorphs from silica ooze to opal-A, opal-CT, and quartz (Africano and Bernard, 2000; Okamoto et al., 2010), resulting in massive, very thick, highly silicified rocks, including "vuggy silica" on the wet surfaces, where available groundwater penetrates. This is commonly observed in the Arpatarla and Şapçı quarries.

Zonation patterns and the directional distribution of alteration minerals can be related to mass transfer between minerals and hydrothermal solutions. The morphology of alteration zones is controlled by (A) a fracture-controlled, fluid-dominated system (i.e., convection) and (B) a heat-conductive, rock-dominated system (i.e., conduction) (Utada, 1980; Izawa, 1986). Convective zones should be distributed relatively symmetrically from the center to the periphery, related to temperature and chemical composition of the fluid in contact with the rocks. The size of each zone developed is a function of the volume and flow rate of the solutions and crystallinity and porosity of the rock (Inoue, 1995). Alteration zone morphology is essentially controlled by the distribution of fractures in the system, which can be grouped as funnel, bedform, and mushroom types. When the ascending geothermal waters come into contact with meteoric water, the pH decreases via the following reactions;

$$4SO_2 + 4H_2O = 3SO_4^{2-} + H_2S + 6H^+ = 3H_2SO_4 + H_2S$$

$$H_2S + 2O_2 = SO_4^{2-} + 2H^+$$

$$4SO_2 + H_2S + 4H_2O + 2O_2 = 5SO_4^{2-} + 10H^+.$$

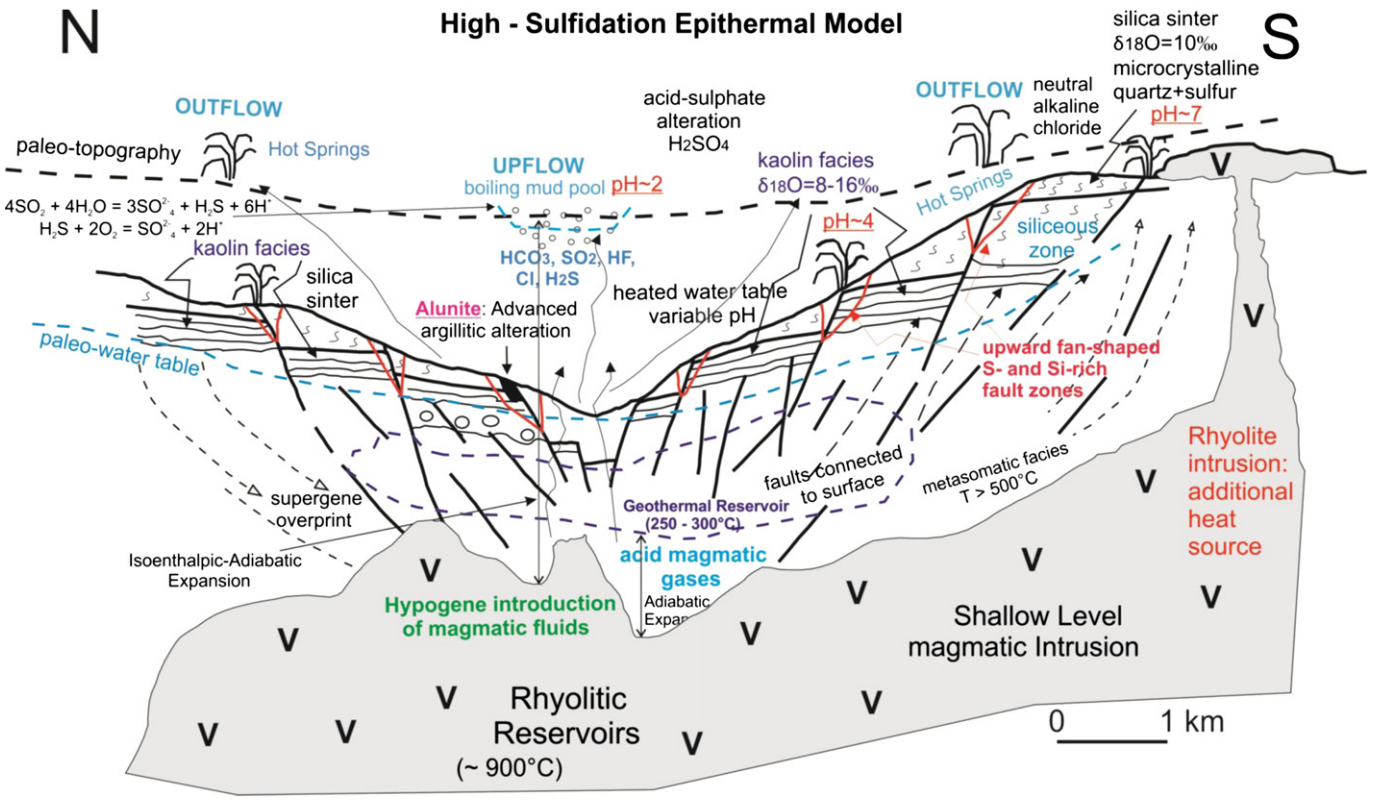

Fig. 14. The proposed fluid- and steam-heated geologic model to explain the origin of high-sulfidization hydrothermal alteration systems for the Düvertepe kaolin district. Modified from Heald et al. (1987), Henley and Ellis (1983) and Cortecci et al. (2001).

Consequently, ascending fluids cause acid-type alteration near the surface. In some case, the subsurface boiling may even bring about a hydrothermal explosion (Hedenquist and Henley, 1985; Hulen and Nielson, 1988). These processes modify the morphology of the alteration zone to form funnel-type morphology and all funnel-type alterations found in the Düvertepe district are as deep as 20 m. The fracture-controlled type hydrothermal alteration is characterized by the development of widespread veins and veinlets in altered rocks (Inoue, 1995), as seen in almost all kaolin deposits in the Düvertepe district (Fig. 3a).

Present geothermal activity gives insight to understanding the evolution of fossil systems found here and in similar fracture systems driven by higher than normal heat flow in thin continental crust, such as the Basin and Range Province, USA and Western Turkey (Hochstein et al., 1990). In a heat conduction-controlled system, rock-dominated type alteration zones are adjacent to the contact of a heat source, such as in an intrusive body. The alteration zones are delineated subparallel to the stratigraphic boundaries by a deep magmatic heat source developed, like that found along the Simav Graben. Turkey also has many present-day low to moderate temperature geothermal fields suitable for power generation (Serpen and Mihçakan, 1999). These fluid convections occur in narrow fracture zones proximal to more normal geothermal gradient environments (Kassoy and Zebib, 1978). The Simav geothermal system is driven by higher than normal heat flow, which, today, is 110 mW/m^2 (İlkışık, 1995). The Simav fault penetrates deep to communicate a deep heat sweep of naturally convecting meteoric waters in metamorphic crust. At the western end of Simav Graben, the presently active Hisaralan Geothermal Field is discharging boiling waters as geysers at the surface. This field is located 10 km west of Düvertepe kaolin district at the northern part of Simav Fault. Near the town of Simav, the Simav fault has a slip of 1000 m on the southern flank. Presently active Eynal, Çitgöl and Naşa Hot Springs discharge at the northern flank of Simav Graben along the Eynal and Naşa faults. This deep fault appears to play an important role in formation of Simav Graben geothermal systems. Both conductive and convective fractured heat types of hydrothermal alteration have been responsible for the evolution of the Düvertepe hydrothermal systems.

The vertical zonation in the quarries is characterized by siliceous sinters at the top, kaolinite–alunite–quartz in the central part, and partly altered tuffs in the lower part. This type of zonation suggests a major structural control of the fluid flow and minor lithological control, which is similar to kaolin mineralization in the western Sardinia, Italy (Simeone et al., 2005). The Simav Graben and surrounding areas have been one of the most tectonically active areas in the Aegean Region. Recent earthquakes in 1955 in the western part of Simav Graben and underneath the town of Simav in May 19th, 2011 (magnitude of 5.9) provide such evidence.

Tuffs are strongly hydrothermally altered due to their glassy composition, high porosity, and high permeability. Their rapid dissolution is attributed to ion exchange, preferential alteration of glass matrices, and dissolution of submicron particle sizes (Bloom and Nater, 1991). During low pH (~3.1) dissolution of glass-rich tuffs, elements are preferentially released in the order Si > Ca > Al > Mg > P. In allophane-rich tuffs at pH = 3.1, the order is Ca > Mg = Si = P > Al due to the original paucity of Ca (Silber et al., 1999). The tuff compositions affect the dissolution rate of Si compared to that of Al, where more Si is dissolved in low pH geothermal waters while passing through rhyolites–dacites and tuffs at depth. These Si-rich geothermal waters eventually spray out as geysers at the surface causing large silica sinter deposits on the Düvertepe kaolin deposits (Fig. 4). There is a positive relation between the size of silica sinters and the size of underlying kaolin deposits due to infiltration effects of volume and splaying geothermal waters.

Yellowstone and New Zealand (Hedenquist and Henley, 1985; Fournier, 1989) offer an analog to the hydrothermal alteration in the Düvertepe kaolin district, where it is possible to propose that boiling was common in shallow levels of the hydrothermal system. Two different types of boiling defined in Yellowstone include: (1) adiabatic boiling, caused by gradual decompression of a slowly ascending, approximately hydrostatic column of water at boiling temperature, and (2) sudden decompressional boiling, caused by an abrupt decrease in pressure on water at or near boiling temperature. Sudden decompressional boiling model appears to be more effective than adiabatic boiling in explaining enrichment in O^{18} and silica in residual water (Sturchio et al., 1990) and is more applicable to the Düvertepe district. The system propagates through the fractures and breccias with sudden flashing of hot water to steam in response to sudden release of pressure by the hydrothermal drainage system along the Simav Graben. This pressure release mechanism involves geyser eruptions (White, 1967), which is about 10 km west of the Düvertepe district. There are active and ancient geysers in the Hisaralan Hot Spring area. We also observe ~2 m high by ~50 cm wide chimneys often containing calcite precipitation.

Fournier and Potter (1982) suggest that quartz-saturated water at 200 °C (~265 mg/l SiO_2) can be enriched in silica through contact with α-cristobalite level (solubility ~464 mg/l SiO_2). So, every ~5 kg of this water would be capable of precipitating 1 g of quartz. Isothermal supersaturation in quartz and clay minerals would be maximized through contact of quartz-saturated water with obsidian, because of its relatively rapid dissolution and relatively high solubility (Sturchio et al., 1990). Quartz-saturated water at 200 °C can be enriched in silica through contact with obsidian to about the level of amorphous silica saturation (~944 mg/l SiO_2), where ~1.5 kg of this water could precipitate 1 g of quartz. This model explains the occurrence of ~50 m thick silica sinter masses in the south of Arpatarla–Şapçı quarries and the Karaağaçli Hill area (Fig. 3) is surrounded by very fresh rhyolites. It is possible that large glass-rich rhyolite reservoir is deeper in the graben (Fig. 3) and they intruded through a secondary volcanic neck providing a source of silica inputs. Based on our field and mineralogical studies, the proposed geologic (steam and fluid-heated) model for the Düvertepe kaolin district is summarized in Fig. 14.

Sillitoe (1993) first recognized the importance of the paleo-water table in shallow epithermal systems and he identified three important factors controlling the changing position of the water table: (1) the presence of porous horizons and subsequent silicification; (2) a falling potentiometric surface during mineralization, which thereby overprints an acid-leached zone onto precious-metal-bearing veins; and (3) intersection of the potentiometric surface at topographic depressions, thus giving rise to hot springs and silica sinter accumulation. By using this scenario, the kaolinitization in the Düvertepe district mostly occurred at or above the paleo-water table (Fig. 14). The boiling of ascending fluids along fracture systems results in formation of acid magmatic volatiles and H_2S-bearing steam that condenses into cool and oxidized groundwater; SO_2 and H_2S oxidation to sulfate forms acidic solutions, which alter the volcanic rocks in the vadose zones above paleo-water tables (Sillitoe, 1993). The existence of thick silica sinters and many silicified rocks along fracture systems in the Düvertepe district leads us to conclude that the position of paleo-water table was more likely close to the surface during the kaolinization. The resulting steam-heated acidic fluids cause advanced argillic alteration with a characteristic powdery, porous texture called "sponge" or "vuggy" silica. Silica sinter is the end-product of intense acid leaching, as described by White et al. (1964) for the Silica Pit at Steamboat, Nevada.

The $\delta^{18}O$ values of hydrothermal silica minerals and in-situ temperature measurements from Yellowstone drill cores (Fig. 2 in Sturchio et al., 1990) showed that quartz forms between 170 and 200 °C and its chalcedony form precipitates between 80 and 200 °C. The range in δO^{18} of the Yellowstone silica minerals is −7.5 to +2.8‰, while Yellowstone meteoric water is about −15‰. The average silica minerals from Düvertepe district are more enriched up to +10‰. It is possible that the silica samples precipitated from Miocene thermal water enriched in $\delta^{18}O$ by hydrothermal processes that include boiling and rock–water exchange.

All studied samples contain microcrystalline quartz. No opal (amorphous silica) was detected, except in the alunite samples. Based on Sturchio et al.'s (1990) studies, this suggests that the temperatures of geothermal water were above 170 °C at the time of hydrothermal alteration. This temperature estimate is supported by the presence of alunite mineralization, which forms at about 200 to 250 °C in upflow area of the same system, where upward fan-shaped Si- and S-rich fault zones occur close to the surface. Opal-CT is only found associated with alunites from Inüstü Hill area during the XRD studies. It is well-known that silica undergoes transformation through time, for example Herdianita et al. (2000) reported that silica older than ~50,000 years have recrystallized to microcrystalline quartz. With the onset of quartz crystallization at ~20,000 years, total water is <0.2 wt.% and porosity is <4%. Since the volcanism is Early Miocene, one might ask how long to expect opal to remain stable? There are many presently active hot springs along the Simav Graben, so it is possible to suggest that minor hydrothermal flows continued through inside alunite mineralization in the Inüstü Hill area during Holocene and those fluids and they are responsible for opal precipitation. This interpretation matches the large statistical deviations in Ar/Ar datings of alunite samples we observed from the north of the graben.

The concentration of silica in hydrothermal systems above 140 °C is generally controlled by quartz solubility (Fournier, 1985). Siliceous hot-spring deposits (sinter) are chemical sediments of noncrystalline silica (opal-A), deposited by near-neutral alkali-chloride waters, derived from deep reservoirs with temperatures > 175 °C (Fournier and Rowe, 1966). During silica diagenesis, metastable forms of silica undergo ordering or recrystallization with time to more stable (less soluble) forms (Murata et al., 1977; Fournier, 1985). The present day geothermal activity is obviously unconnected to the Early Miocene kaolinization processes, but it gives general idea about the genesis of kaolin deposits. Using O-isotope values of kaolinite, silica sinter precipitated at 79–83 °C. Three samples in Şapçı show temperatures above 110 °C, two samples in Arpatarla show ~00 °C and Doren samples range from 65 to 129 °C (Table 4). These calculated formation temperatures explain why only micro quartz precipitated together with kaolinites. Based on geochemical assessment of Simav geothermal waters (Eynal, Çitgöl and Naşa hot springs), quartz and Na–K geothermometers were used to calculate the reservoir temperatures as 70–195 °C and 167–249 °C, respectively, and the Na–K–Mg geothermometer indicated temperatures of approximately 230–240 °C (Palabiyik and Serpen, 2008). The Simav geothermal reservoir is ^{18}O enriched and is fed by Nadarçam cold spring. The ^{18}O of geothermal waters range from −9.6‰ to −8.9‰ indicating >100 °C reservoir temperature. This points to the existence of fluid–rock interaction in the system and/or boiling in the reservoir. Consequently, $\delta^{18}O$ enrichment should be expected in kaolinites in the Düvertepe samples (Table 2). The alteration mineralogy of rock samples collected at the Simav geothermal region indicates that chlorite, albite, K-feldspar, epidote, muscovite, illite and montmorillonite are probably in equilibrium with geothermal water and that the reservoir temperatures are between 160 °C and 250 °C (Palabiyik and Serpen, 2008).

Using the silica geothermometers, Fournier's (1977) quartz-maximum evaporation (88–177 °C), Fournier and Potter's (1982) quartz-adiabatic cooling (86–179 °C), and Arnorsson's (2000) quartz (70–184 °C) geothermometers yielded a temperature range of 70–184 °C, indicating temperatures that are likely to be close to actual reservoir and bottom-hole temperatures of the Simav geothermal reservoirs (Palabiyik and Serpen, 2008). Fournier's (1977) quartz (85–191 °C), Fournier and Potter's (1982) quartz (85–192 °C), Verma and Santoyo's (1997) quartz (85–192 °C) and Verma's (2000) quartz (78–195 °C) geothermometers suggest a temperature range of 78–195 °C, indicating a reservoir temperature approximately 10 °C higher than those proposed by Palabiyik and Serpen (2008).

9. Conclusions

This study of kaolin and alunite deposits and hypogene metasomatism of the Düvertepe district constraints it origins to a model of fluid- and steam-heated magmatic–hydrothermal system. Kaolinite (±alunite) mineralization mostly occurs in the intersections of one or more major faults, which trend almost perpendicular to the Simav Fault (Bağkıran Hill, Arpatarla Hill, Cehennem Hill). Major kaolin deposits are associated with the major fault zones that provide S- and Si-rich hydrothermal waters. Mineral assemblages from the north and south of the graben are similar. The only difference is that alunite is more concentrated in certain areas in the north of the graben.

FE-SEM and petrographic studies show that the presence of volcanic glass was more influential than the feldspars during the alteration of rhyolites–rhyodacites and tuffs. It is possible to suggest that majority of the Düvertepe kaolinite (±alunite) deposits occurred from volcanic glass alteration. Petrographic studies reveal that there are insufficient feldspar sources in the volcanic rocks and tuffs to increase the occurrence of kaolin. A significant part of parent material was volcanic glass in the Düvertepe kaolin district. Additional XRD and TGA data reveal two different mineral paragenetic groups defined as kaolinite + quartz + alunite (kaolin-type) and as alunite + opal-CT + quartz (alunite-type). Mineralogical assemblages in the Doren kaolin quarry samples are found as kaolinite, alunite and quartz in the north of the graben.

Siliceous rocks and silica sinters are the striking features for the exploration of large hydrothermal kaolin deposits in the Düvertepe district, as seen in the Kabaağaçlı and Arpatarla hills along the west side of the respective NW–SE and NE–SW trending fault zones. Flashing and infiltration of hydrothermal solutions on the surface caused precipitation of silica minerals as a result of sudden dropping of hydrostatic pressure. As a result, quality of kaolin reserves improves underneath the silica. It is observed that the thickness of siliceous rocks reaches up to 50 m in south of the graben.

Table 4
Hydrothermal alteration features at Düvertepe kaolin district.
Modified from Simeone et al., 2005.

Alteration facies	Spatial distribution	Genetic process involved
Massive silicified masses	>50 m thick in south of Arpatarla deposit at main fault zone	Silica deposition and replacement by cooling of ascending geothermal waters
Siliceous veins along fault zones	Fill fractures at almost all kaolin quarries	Cooling of ascending geothermal waters at water table. Sulfur contents are always high.
Massive alunite body + opal-CT + quartz	Widely distributed alteration mineral at Inüstü Tepe.	High-sulfide acid alteration of volcanic tuffs. Upflow area of SO_4-rich hydrothermal fluid.
Siliceous layers, quartz nodules and cobbles	Commonly found in various horizons within kaolin bodies	Late-stage alteration of volcanic tuffs
Kaolinite 1 T, ±alunite, ±quartz	North and south of Simav graben along main fault zone	Replacement (chemical leaching) of rhyolitic–rhyodacitic tuffs
Montmorillonite, kaolinite 1 Md, quartz	Distal alteration of neutral geothermal water at bentonite deposit	Replacement (chemical leaching) of rhyolitic–rhyodacitic tuffs
Kaolinite 1 T, quartz, alunite	Far away from kaolin deposits interlayer with kaolinite in both sided of small fault	Replacement (strong leaching) of rhyolitic–rhyodacitic tuffs

Sulfur isotopes suggest that sulfate content of acidic geothermal waters has meteoric and magmatic origin. Oxygen and hydrogen values of kaolinite minerals also suggest deep circulation of hydrothermal system due to opening of the graben. Geochronological studies using K–Ar and Ar–Ar dating reveal that geothermal activity initiated in south of the graben about 2–3 Ma years before the north of the graben during Early Miocene. It is postulated that chemical composition of hydrothermal fluids was more enriched with dissolved silica content at formation temperatures between 50 and 120 °C, which were higher during the initial stage of hydrothermal activity. In terms of timing of mineralization events, alunite precipitated at high temperature around 280 °C and kaolinite precipitated later at low temperature below 100 °C.

It is proposed herein that silica- and sulfate-rich ascending acidic geothermal waters rose along major and minor fault zones and caused silica precipitation between altered rhyolite–rhyodacitic tuffs and kaolinizied zones. When the rising of saturated cation- and anion-rich ascending geothermal waters along fault zones gets close to the surface, pressure and temperature drop, and spray over the volcanic tuffs, and consequently, excess silica precipitated in those areas where they reached the surface.

Acknowledgments

This research is made possible with the support of TÜBİTAK-ÇAYDAG Project No: 106Y070 (Ö.I. Ece). Additional support was obtained from the Istanbul Technical University Research Fund (BAP Project No: 32382) (Ö.I. Ece). We express our gratitude to Gültekin Göller for providing technical support during FE-SEM studies in Istanbul Technical University, to Marion J. Wampler for K–Ar dating analyses in Georgia State University and to Chris Hall for $^{40}Ar/^{39}Ar$ studies in the University of Michigan, Ann Arbor. Also, we express our gratitude to Kalemaden Mining Corp. for their logistic support and accommodations during the field work in the summers of 2007 and 2008. We are indebted to Jeffrey L. Mauk and Robert L. Brathwaite of the University of Auckland, and Byron R. Berger of the USGS for their time devoted to reviewing an early version of this manuscript.

Appendix A. Supplementary data

Supplementary data to this article can be found online at http://dx.doi.org/10.1016/j.jvolgeores.2013.01.012.

References

Africano, F., Bernard, A., 2000. Acid alteration in the fumarolic environment of Usu volcano, Hokkaido, Japan. Journal of Volcanology and Geothermal Research 97, 475–495.
Africano, F., van Rompaey, G., Bernard, A., Le Guern, F., 2002. Deposition of trace elements from high temperature gases at Satsuma-Iwojima volcano. Earth and Planetary Space 54, 275–286.
Akay, E., 2008. Geology and petrology of the Simav Magmatic Complex and its comparison with the Oligo–Miocene granitoids in NW Anatolia: implications on Tertiary tectonic evolution of the region. International Journal of Earth Sciences 98, 1655–1675.
Akdeniz, N., Konak, N., 1979. Menderes Masifi'nin Simav dolayındaki kaya birimleri ve metabazik metaultrabazik kayaların konumu. Turkish Geological Society (TJK) Bulletin 22, 175–184.
Altaner, S.P., Ylagan, R.F., Savin, S.M., Aronson, J.L., Belkin, H.E., Pozzuoli, A., 2003. Geothermometry, geochronology, and mass transfer associated with hydrothermal alteration of a rhyolitic from Ponza Island, Italy. Geochimica et Cosmochimica Acta 67, 275–288.
Altunkayanak, S., Dilek, Y., 2006. Timing and nature of postcollisional volcanism in western Anatolia and geodynamic implications. Geological Society of America Special Paper 409, 321–351.
Altunkaynak, Ş., Genç, C., 2008. Petrogenesis and time-progressive evolution of the Cenozoic continental volcanism in the Biga Peninsula, NW Anatolia (Turkey). Lithos 102, 316–340.
Altunkaynak, S., Dilek, Y., Genç, S.C., Sunal, G., Gertisser, R., Furnes, H., Foland, K.A., Yang, J., 2012. Spatial, temporal and geochemical evolution of Oligo–Miocene granitoid magmatism in western Anatolia, Turkey. Gondwana Research 21, 961–986.
Arnorsson, S., 2000. Isotopic and Chemical Techniques in Geothermal Exploration, Development and Use. International Atomic Energy Agency, Vienna, pp. 156–187.
Arribas Jr., A., 1995. Characteristics of high-sulfidation epithermal deposits, and their relation to magmatic fluid. Mineralogical Association of Canada Short Course 23, 419–454.
Arribas, A., Arribas, I., Draper, G., Hall, C., Kesler, S.E., McEwan, C., Muntean, J.L., 2011. $^{40}Ar/^{39}Ar$ dating of alunite from the Pueblo Viejo gold–silver district, Dominican Republic. Economic Geology 106, 1059–1070.
Babcock, R.S., 1973. Computational models of metasomatic processes. Lithos 6, 279–290.
Bloom, P.R., Nater, E.A., 1991. Kinetics of dissolution of oxide and primary silicate minerals. In: Sparks, D.L., Suarez, D.L. (Eds.), Rates of Soil Chemical Processes: Soil Science Society of America Book Series (Madison), pp. 151–189.
Bozkurt, E., 2001. Neotectonics of Turkey — a synthesis. Geodinamica Acta 14, 3–30.
Bozzola, J.J., Russell, L.D., 1999. Electron Microscopy: Principles and Techniques for Biologists. Jones and Bartlett Publishers, Boston, p. 670.
Browne, P.R.L., Ellis, A.J., 1970. The Ohaaki–Broadlands–Ohaaki geothermal area, New Zealand: mineralogy and related geothermal. American Journal of Science 269, 97–131.
Chouinard, A., Williams-Jones, A.E., Leonardson, R.W., Hodgson, C.J., Silva, P., Tellez, J.V., Rojas, F., 2005. Geology and genesis of the multistage high-sulfidation epithermal Pascua Au–Ag–Cu deposit, Chile and Argentina. Economic Geology 100, 463–490.
Çoban, H., Karacık, Z., Ece, Ö.I., 2012. The role of slab roll-back and extensional collapse on the generation of coexisting early to middle Miocene alkaline and calc-alkaline back-arc magmas in western Anatolia extensional province; a record from Simav (Uşak) region, Turkey. Lithos 140–141, 119–141.
Cortecci, G., Dinelli, E., Bolognesi, L., Boschetti, T., Ferrara, G., 2001. Chemical and isotopic compositions of water and dissolved sulfate from shallow wells on Vulcano Island, Aeolian Archipelago, Italy. Geothermics 30, 69–91.
Cunningham, C.G., Rasmussen, J.D., Steven, T.A., Rye, R.O., Rowley, P.D., Romberger, S.B., Selverstone, J., 1998. Hydrothermal uranium deposits containing molybdenum and fluorite in the Marysvale volcanic field, west-central Utah. Mineralium Deposita 33, 477–494.
Demirhan, M., 1986. A report on kaolin occurrences in Kütahya–Emet, Simav, Altıntaş and Balıkesir–Sındırgı, Düvertepe region. General Directorate of Mineral Research and Exploration (MTA) Report No: 7894 (in Turkish, open-file report).
Dilek, Y., Altunkaynak, S., 2010. Geochemistry of Neogene–Quaternary alkaline volcanism in western Anatolia, Turkey, and implications for the Aegean mantle. International Geology Review 52, 631–655.
Dilek, Y., Altunkaynak, S., Öner, Z., 2009. Syn-extensional granitoids in the Menderes core complex and the late Cenozoic extensional tectonics of the Aegean province. In: Ring, U., Wernicke, B. (Eds.), Extending a Continent: Architecture, Rheology and Heat Budget: Geological Society, London, Special Publications, 321, pp. 197–223.
Dill, H.G., Bosse, H.R., Henning, K.H., Fricke, A., 1997. Mineralogical and chemical variations in hypogene and supergene kaolin deposits in a mobile fold belt the Central Andes of Northwestern Peru. Mineralium Deposita 32, 149–163.
Ece, Ö.I., Nakagawa, Z., 2003. Alteration of volcanic rocks and genesis of kaolin deposits in Şile Region, Northern Istanbul, Turkey. Part — II. Differential mobility of elements. Clay Minerals 38, 529–550.
Ece, Ö.I., Schroeder, P.A., 2007. Clay mineralogy and chemistry of halloysite and alunite deposits in the Turplu area, Balıkesir, Turkey. Clays and Clay Minerals 55, 18–35.
Ece, Ö.I., Schroeder, P.A., Smilley, M.J., Wampler, J.M., 2008. Acid-sulfate hydrothermal alteration of andesitic tuffs and genesis of halloysite and alunite deposits in the Biga Peninsula, Turkey. Clay Minerals 43, 281–315.
Faure, G., 1986. Principles of Isotope Geology, 2nd ed. Wiley, New York.
Fournier, R.O., 1977. Chemical geothermometers and mixing models for geothermal systems. Geothermics 5, 41–50.
Fournier, R.O., 1985. The behaviour of silica in hydrothermal solution. In: Berger, B.R., Bethke, P.M. (Eds.), Geology and Geothermal of Epithermal Systems: Society of Economic Geology Reviews in Economic Geology, 2, pp. 45–72.
Fournier, R.O., 1989. Geochemistry and dynamics of the Yellowstone National Park hydrothermal system. Annual Review of Earth and Planetary Sciences 17, 13–53.
Fournier, R.O., Potter, R.W., 1982. A revised and expanded silica quartz geothermometer. Geotherm Resource Council Bulletin 11, 3–12.
Fournier, R.O., Rowe, J.J., 1966. Estimation of underground temperatures from the silica content of water from hot springs and steam wells. American Journal of Science 264, 685–697.
Gat, J.R., Carmi, I., 1970. Evolution in the isotopic composition of atmospheric waters in the Mediterranean Sea area. Journal of Geophysical Research 75, 3039–3048.
Gifkins, C., Herrmann, W., Large, R., 1995. Altered Volcanic Rocks. A Guide to Description and Interpretation. University of Tasmania, Australia (275 pp.).
Giggenbach, W.F., 1984. Mass transfer in hydrothermal alteration systems — a conceptual approach. Geochimica et Cosmochimica Acta 48, 2693–2711.
Giggenbach, W.F., 1988. Geothermal solute equilibria: derivation of Na–K–Mg–Ca geoindicators. Geochimica et Cosmochimica Acta 52, 2749–2765.
Gilg, H.A., Weber, B., Kasbohm, J., Frei, R., 2003. Isotope geochemistry and origin of illite–smectite and kaolinite from the Seiltz and Kemmlitz kaolin deposits, Saxony, Germany. Clay Minerals 38, 95–112.
Görür, N., Tüysüz, O., 2001. Cretaceous to Miocene palaeogeographic evolution of Turkey implications for hydrocarbon potential. Journal of Petroleum Geology 24, 119–146.
Görür, N., Şengör, A.M.C., Sakınç, M., 1995. Rift formation in the Gökova region, southwest Anatolia — implications for the opening of the Aegean Sea. Geological Magazine 132, 637–650.
Grant, J.A., 1986. The isochron diagram — a simple solution to Gresen's equation for metasomatic alteration. Economic Geology 81, 1976–1982.
Gresens, R.L., 1967. Composition–volume relationship of metasomatism. Chemical Geology 2, 47–65.
Harris, C., Compton, J.S., Bevington, S.A., 1999. Oxygen and hydrogen isotope composition of kaolinite deposits, Cape Peninsula, South Africa; low-temperature, meteoric origin. Economic Geology 94, 1353–1366.

Hayashi, M., 1973. Hydrothermal alteration in the Otake geothermal area, Kyushu. Journal of Japan Geothermal Energy Association 10, 9–46.
Hayba, D.O., Bethke, P.M., Heald, P., Faley, N.K., 1985. Geologic, mineralogic and geochemical characteristics of volcanic-hosted epithermal precious-metal deposits. Reviews in Economic Geology 2, 129–167.
Heald, P., Foley, N.K., Hayba, D.O., 1987. Comparative anatomy of volcanic-hosted epithermal deposits: acid-sulphate and adularia–sericite types. Economic Geology 82, 1–26.
Hedenquist, J.W., Henley, R.W., 1985. Hydrothermal eruptions in the Waiotapu geothermal system, New Zealand: their origin, associated breccias, and relation to precious metal mineralization. Economic Geology 80, 1640–1668.
Hedenquist, J.W., Matsuhisa, Y., Izawa, E., White, N.C., Giggenbach, W.F., 1994. Geology, geochemistry, and origin of high sulphidation Cu–Au mineralization in the Nansatsu District, Japan. Economic Geology 89, 1–30.
Hemley, J.J., Hostetler, P.B., Gude, A.J., Mountjoy, W.T., 1969. Some stability relations of alunite. Economic Geology 64, 599–611.
Hemley, J.J., Montoya, J.W., Marinenko, J.W., Luce, R.W., 1980. Equilibria in the system Al_2O_3–SiO_2–H_2O and some general implications for alteration/mineralization processes. Economic Geology 75, 210–228.
Henley, R.D., Berger, B.R., 2011. Magmatic-vapor expansion and the formation of high-sulfidation gold deposits: chemical controls on alteration and mineralization. Ore Geology Reviews 39, 63–74.
Henley, R.D., Ellis, A.J., 1983. Geothermal systems ancient and modern: a geochemical review. Earth-Science Reviews 19, 1–50.
Herdianita, N.R., Browne, P.R.L., Rodgers, K.A., Campbell, K.A., 2000. Mineralogical and textural changes accompanying ageing of silica sinter. Mineralium Deposita 35, 48–62.
Hinckley, D.N., 1963. Variability in "crystallinity" values among the kaolin deposits of the coastal plain of Georgia and South Carolina. Clays Clay Miner 11, 229–235.
Hochstein, M.P., Zhongke, Y., Ehara, S., 1990. The Fuzhou geothermal system (People's Republic of China): modelling study of a low temperature fracture-zone system. Geothermics 19, 43–60.
Holland, H.D., 1965. Some applications of thermochemical data to problems of ore deposits, II. Mineral assemblages and the composition of ore-forming fluids. Economic Geology 60, 1101–1166.
Holland, H.D., 1967. Gangue minerals in hydrothermal deposits. In: Barnes, H.L. (Ed.), Geochemistry of Hydrothermal Ore Deposits. Holt, Rinehart and Winston, New York, pp. 382–436.
Hulen, J.B., Nielson, D.L., 1988. Hydrothermal brecciation in the Jemez fault zone: Valles Caldera, New Mexico: results from continental scientific drilling program core hole VC-1. Journal of Geophysical Research 93, 6077–6090.
Hüsing, S.K., Zachariasse, W., Van Hinsbergen, D.J.J., Krijgsman, W., Inceöz, M., Harzhauser, M., Mandic, O., Kroh, A., 2009. Oligocene–Miocene basin evolution in SE Anatolia, Turkey: constraints on the closure of the eastern Tethys gateway. In: Van Hinsbergen, D.J.J., Edwards, M.A., Govers, R. (Eds.), Collision and Collapse at the Africa–Arabia–Eurasia Subduction Zone: The Geological Society, London, Special Publications, 311, pp. 107–132.
Inoue, A., 1995. Formation of clay minerals in hydrothermal environments. In: Velde, B. (Ed.), Origin and Mineralogy of Clays. Springer-Verlag, Berlin, p. 333.
Iwao, S., 1968. Zonal structure in some kaolin and associated deposits of hydrothermal origin in Japan. Proceedings of 23rd International Geological Congress, 14, pp. 107–113.
Izawa, S., 1986. Clay minerals in epithermal deposits. J Mineral Society Japan Special Paper Issue 17, 17–24.
İlkışık, M., 1995. Regional heat flow in Western Anatolia using silica temperature estimates from thermal springs. Tectonophysics 244, 175–184.
Justet, L., Spell, T.L., 2001. Effusive eruptions from a large silicic magma chamber: the Bearhead Rhyolite, Jemez volcanic field, NM. Journal of Volcanology and Geothermal Research 107, 241–264.
Kassoy, D.R., Zebib, A., 1978. Convection fluid dynamics in a model of a fault zone in the earth crust. Journal of Fluid Mechanics 88, 769–792.
Keller, W.D., Hanson, R.S., 1968. Hydrothermal alteration of a rhyolite flow breccias near San Luis Potasi, Mexico. Clays and Clay Minerals 16, 223–229.
Keller, W.D., Hanson, R.S., 1969. Hydrothermal argillation of volcanic pipes in limestone in Mexico. Clays and Clay Minerals 17, 9–12.
Köster, H., 1974. Ein beitrag zur geochemie und enstehung der oberpfabzischen kaolin–feldspat–lagerstatten. Geologische Rundschau 63, 655–689.
Kyle, J.E., Schroeder, P.A., Wiegel, J., 2007. Microbial silicification in sinters from tow terrestrial hot springs in the Uzon Caldera, Kamchatka, Russia. Geomicrobiology Journal 24, 627–641.
Love, D.A., Clark, A.H., Jay Hodson, C., Mortensen, I.K., Archibald, D.A., Farrar, E., 1998. The timing of adularia-sericite-type mineralization and alunite-kaolinite-type alteration, Mount Skukum epithermal gold deposit, Yukon Territory, Canada: $^{40}Ar/^{39}Ar$ and U-Pb geochronology. Economic Geology 93, 437–462.
MacLean, W.I., Kranidiotis, P., 1987. Immobile elements as monitors of mass transfer in hydrothermal alteration: Phelps Dodge massive sulfide deposit, Matagami, Quebec. Economic Geology 82, 951–962.
Madeisky II, E., 1996. A lithogeochemistry and radiometric study of hydrothermal alteration and metal zoning at the Cinola epithermal gold deposit, Queen Charlotte Islands, British Columbia. In: Coyner, A.R., Fahey, P.L. (Eds.), Geology and Ore Deposits of the Cordillera 3, 1153–1185.
Maksimovic, Z., Panto, G.Y., 1983. Mineralogy of yttrium and lanthanide elements in karstic bauxite deposits. Travaux ICSOBA 18, 191–200.
Murata, K.J., Friedman, I., Gleason, J.D., 1977. Oxygen isotope relations between diagenetic silica minerals in Monterey Shale, Temblor Range, California. American Journal of Science 277, 259–272.
Mutlu, H., Sarıız, K., Kadir, S., 2005. Geochemistry and origin of the Şaphane alunite deposit, Western Anatolia, Turkey. Ore Geology Reviews 26, 39–50.
Nesbitt, H.W., Young, G.M., 1982. Early Proterozoic climates and plate motions inferred from major element chemistry of lutites. Nature 279, 715–717.
Nesbitt, H.W., Young, G.M., 1984. Prediction of some weathering trends of plutonic and volcanic rocks based on thermodynamic and kinetic considerations. Geochimica et Cosmochimica Acta 48, 1523–1534.
Ohmoto, H., 1972. Systematics of sulfur and carbon isotopes in hydrothermal ore deposits. Economic Geology 67, 551–579.
Ohmoto, H., Rye, R.O., 1979. Isotopes of sulfur and carbon. In: Barnes, H.L. (Ed.), Geochemistry of Hydrothermal Ore Deposits. Holt, Rinehart and Winston, New York, pp. 509–567.
Okamoto, A., Saishu, H., Hirano, N., Tsuchiya, N., 2010. Mineralogical and textural variation of silica minerals in hydrothermal flow-through experiments: implications for quartz vein formation. Geochimica et Cosmochimica Acta 74, 3692–3706.
Okay, A.I., Siyako, M., Burkan, K.A., 1991. Geology and tectonic evolution of the Biga Peninsula, northwest Turkey. Bulletin of Istanbul Technical University 44, 191–256.
Okay, A.I., Demirbağ, E., Kurt, H., Okay, N., Kuşçu, I., 1999. An active, deep marine strike–slip basin along the North Anatolian Fault in Turkey. Tectonics 18, 129–147.
Okay, A., Kaşlılar-Özcan, A., İmren, C., Boztepe-Güney, A., Demirbağ, E., Kuşçu, I., 2000. Active faults and evolving strike–slip basins in the Marmara Sea, northwest Turkey: a multichannel seismic reflection study. Tectonophysics 321, 189–218.
Oygür, V., 1997. Anatomy of an epithermal mineralization: Mumcu (Balıkesir–Sındırgı), inner-western Anatolia, Turkey. Mineral Research and Exploration Bulletin 119, 29–39.
Oygür, V., Erler, A., 2000. Comparison of the epithermal and base-metal mineralizations along the Simav graben. Proceedings 52nd Geological Congress of Turkey May 1999 Ankara 12–13.
Palabiyik, Y., Serpen, U., 2008. Geochemical assessment of Simav Geothermal Field, Turkey. Revista Mexicona de Ciencias Geologicas 25, 408–425.
Railsback, L.B., 2003. An earth scientist's periodic table of the elements and their ions. Geology 31, 737–740.
Rye, R.O., Bethke, P.M., Wasserman, W.D., 1992. The stable isotope geochemistry of acid sulfate alteration. Economic Geology 87, 225–262.
Sakai, H., Matsubaya, O., 1977. Stable isotope studies of Japanese geothermal systems. Geothermics 5, 97–124.
Sayın, S.A., 1984. The role of hydrogen-metasomatism in the hydrothermal kaolin occurrences, Gönen, western Turkey. Key Engineering Materials 264–268, 1379–1382.
Sayın, S.A., 2007. Origin of kaolin deposits: evidence from the Hisarcık (Emet–Kütahya) deposits, Western Turkey. Turkish Journal of Earth Sciences 16, 77–96.
Schroeder, P.A., Shiflet, J., 2000. Ti-bearing phases in the Huber Formation, an east Georgia kaolin deposits. Clays and Clay Minerals 48, 151–158.
Serpen, U., Mihçakan, M., 1999. Heat flow and related geothermal potential of Turkey. In: Geothermal Resources Council (GRC). Annual Meeting, GRC Transactions, 23, pp. 485–490.
Seyitoğlu, G., 1997. The Simav Graben: an example of young E–W trending structures in the Late extensional system of Western Turkey. Turkish Journal of Earth Sciences 6, 135–141.
Seyitoğlu, G., Scott, B.C., 1992. The age of the Büyük Menderes Graben (West Turkey) and its tectonic implications. Geological Magazine 129, 239–242.
Sheppard, S.M.F., Gilg, H.A., 1996. Stable isotope geochemistry of clay minerals. Clay Minerals 31, 1–24.
Silber, A., Bar-Yusuf, B., Chen, Y., 1999. pH-dependent kinetics of tuffs dissolution. Geoderma 93, 125–140.
Sillitoe, R.H., 1993. Epithermal models: genetic types, geothermal controls and shallow features. In: Kirkham, R.V., Sinclair, W.D., Thorpe, R.I., Duke, J.M. (Eds.), Mineral Deposit Modeling: Geological Association of Canada Special Paper, 40, pp. 403–417.
Sillitoe, R.H., Hedenquist, J.W., 2003. Linkages between volcanotectonic settings, ore fluid compositions and epithermal precious metal deposits. In: Simmons, S.F., Graham, I. (Eds.), Volcanic, Geothermal and Ore-forming Fluids: Ruker and Witnesses of Processes Within the Earth: Society of Economic Geologists Special Publication, 10, pp. 315–343.
Simeone, R., Dilles, J.H., Padalino, G., Palomba, M., 2005. Mineralogical and stable isotope studies of kaolin deposits: shallow epithermal systems of western Sardinia, Italy. Economic Geology 100, 115–130.
Simmons, S.F., Browne, P.R.L., 2000. Hydrothermal minerals and precious metals in the Broadlands–Ohaaki–Ohaaki geothermal system: implications for understanding low-sulfidation epithermal environments. Economic Geology 95, 971–999.
Siyako, M., Bürkan, K.A., Okay, A.I., 1989. Tertiary geology and hydrocarbon potential of the Biga and Gelibolu Peninsulas. Turkish Association of Petroleum Geologists Bulletin 1, 183–199.
Snellings, R., van Haven, T., Machiels, L., Mertens, G., Vandenberghe, N., Elsen, J., 2008. Mineralogy, geochemistry and diagenesis of clinoptilolite tuffs (Miocene) in the Central Simav Graben, Western Turkey. Clays and Clay Minerals 56, 622–632.
Sousa, D.J.L., Varajao, A.F.D.C., Yvon, J., Da Costa, G.M., 2007. Mineralogical, micromorphological and geochemical evolution of the kaolin facies deposit from the Capim region (northern Brazil). Clay Minerals 42, 69–87.
Spell, T.L., McDougall, I., 2003. Characterization and calibration of $^{40}Ar/^{39}Ar$ dating standards. Chemical Geology 198, 189–211.
Staudacher, T., Jessberger, E.K., Dominik, B., 1982. Ar^{40}/Ar^{39} ages of rocks and glasses from the Nordlinger Ries Crater and the temperature history of impact breccias. Journal of Geophysics-Zeitschrift für Geophysik 51, 1–11.
Stoffregen, R.E., 1987. Genesis of acid-sulfate alteration and Au–Cu–Ag mineralization at Summitville, Colorado. Economic Geology 82, 1575–1591.
Stoffregen, R.E., Rye, R.O., Wasserman, M.D., 1994. Experimental studies of alunite: I. 18O-16O and D–H fractionation factors between alunite and water at 250–450 °C. Geochimica et Cosmochimica Acta 58, 903–916.

Sturchio, N.C., Keith, T.E.C., Muehlenbachs, K., 1990. Oxygen and carbon isotope ratios of hydrothermal minerals from Yellowstone drill cores. Journal of Volcanology and Geothermal Research 40, 23–37.

Şengör, A.M.C., 1985. The Alpides and Kimmerides - The doubled history of problems and prospects. Geologische Rundschau 74, 181–213.

Taylor, H.P., 1979. Oxygen and hydrogen relationships in hydrothermal mineral deposits. In: Barnes, H.L. (Ed.), Geochemistry of Hydrothermal Ore Deposits. 2nd edition. Wiley, New York, pp. 236–277.

Taylor, B.E., 1992. Degassing of H_2O from rhyolite magma during eruption and shallow intrusion, and the isotopic composition of magmatic water in hydrothermal systems. Report of Geological Survey of Japan, No:279, pp. 190–194.

Utada, M., 1980. Hydrothermal alteration related to igneous acidity in Cretaceous and Neogene formations of Japan. Mining Geology of Japan, Special Issue, 8, pp. 67–83.

Uysal, I.T., Golding, S.D., Baublys, K., 2000. Stable isotope geochemistry of authigenic clay minerals from Late Permian coal measures, Queensland, Australia: implication for the evolution of the Bowen Basin. Earth and Planetary Science Letter 180, 149–162.

Uysal, I.T., Mutlu, H., Altunel, E., Karabacak, V., Golding, S.D., 2006. Clay mineralogical and isotopic (K–Ar, $\delta^{18}O$, δD) constraints on the evolution of the North Anatolian Fault Zone, Turkey. Earth and Planetary Science Letter 243, 181–194.

Uz, B., 1985. Akdağ Masifi'nde Simav–Kütahya yeşil şistlerin petrojenik ve kökensel incelemesi. Jeoloji Mühendisliği 23, 21–30.

van Hinsbergen, D.J., Dekkers, M.J., Bozkurt, E., Koopman, M., 2010. Exhumation with a twist: paleomagnetic constraints on the evolution of the Menderes metamorphic core complex, western Turkey. Tectonics 29, TC3009. http://dx.doi.org/10.1029/TC002596.

Vennemann, T.W., Muntean, J.L., Kesler, S.E., O'Neil, J.R., 1993. Stable isotope evidence for magmatic fluids in the Pueblo Viejo epithermal silica–alunite Au–Ag deposit, Dominican Republic. Economic Geology 88, 55–71.

Verma, M.P., 2000. Revised quartz solubility temperature dependence equation along the water–vapor saturation curve. World Geothermal Congress, Kyushu-Tohoku, Japan, pp. 1927–1932.

Verma, S.P., Santoyo, E., 1997. New improved equations for Na/K, Na/Li and SiO_2 geothermometers by outlier detection and rejection. Journal of Volcanology and Geothermal Research 79, 9–23.

Wang, Y., 2010. Physical and chemical characteristics of the host rocks in controlling the mineralization of the Chinkuashih high-sulfidation gold–copper deposits northeastern Taiwan. Journal of Geochemical Exploration 104, 61–68.

Wang, Y., Sasaki, M., Sasada, M., Chen, C.H., 1999. Fluid inclusion studies of the Chinkuashih high-sulfidation gold–copper deposits in Taiwan. Chemical Geology 154, 155–167.

Warren, I., Simmons, S.F., Mauk, J.L., 2007. Whole-rock geochemical techniques for evaluating hydrothermal alteration, mass changes, and compositional gradients associated with epithermal Au–Ag mineralization. Economic Geology 102, 923–948.

White, D.E., 1967. Some principles of geyser activity, mainly from Steam Boat Springs, Nevada. American Journal of Science 265, 641–684.

White, D.C., Thompson, G.A., Sandberg, C.H., 1964. Rocks, Structure, and Geologic History of Steamboat Springs Thermal Area, Washoe County, Nevada. USGS, Professional Paper 458-B. (63 pp.).

Xiangji, L., Fusheng, W., 1998. Experimental study on the formation mechanism of the Fanshan alunite deposit in Pingyang, Zhejiang. Acta Geologica Sinica 1998-02 (http://en.cnki.com.cn/Article_en/CJFDTOTAL-DZXE199802007.htm).

Yau, Y.C., Peacor, D.R., Essene, E.J., 1987. Authigenic anatase and titanite in shales from the Salton Sea Geothermal Field, California. Neues Jahrb Mineral Monatsh 87, 441–452.

Yılmaz, Y., Genç, Ş.C., Gürer, F., Bozcu, M., Yılmaz, K., Karacık, Z., Altunkaynak, Ş., Elmas, A., 2000. When did the western Anatolian grabens begin to develop? In: Bozkurt, E., Winchester, J.A., Piper, J.D.A. (Eds.), Tectonics and Magmatism in Turkey and the Surrounding Area: Geological Society of London Special Publication, 173, pp. 353–384.